



# A Review of Sliding Mode Observer Based Sensorless Control Methods for PMSM Drive

Ying Zuo , *Student Member, IEEE*, Chunyan Lai , *Senior Member, IEEE*,  
and K. Lakshmi Varaha Iyer, *Senior Member, IEEE*

**Abstract**—For permanent magnet synchronous machines (PMSMs), high-performance control strategies rely on sensors to obtain accurate information of rotor position and speed. However, mechanical sensors are expensive and susceptible to harsh environment. Therefore, various sensorless control strategies have been proposed and intensively investigated for decades. Among them, sliding mode observer (SMO) based sensorless control method has drawn increasing attention due to its simple implementation and strong robustness. This article presents a comprehensive review of SMO-based sensorless control strategies for PMSMs reported in the literature. State-of-the-art SMO-based sensorless control strategies have been reviewed and investigated, and the design of SMO under nonideal conditions is presented as well. In addition, future research trends for SMO-based sensorless control strategies are also discussed.

**Index Terms**—Permanent magnet synchronous motors, sensorless control, sliding mode observer (SMO).

## I. INTRODUCTION

PERMANENT magnet synchronous machines (PMSMs) are widely employed in servo control, automotive, aerospace, and wind power generation systems due to its high power density, high efficiency, and simple structure [1], [2], [3]. For improved system performance, high-performance control strategies rely on sensors to obtain accurate information of rotor position and speed. Thus, position sensor such as the optical encoder or a resolver needs to be installed on the machine shaft. The employment of these extra position detecting devices and associated signal processing equipment for position information, on the other hand, is well known to increase costs. In reality, not only is the cost of the position sensor itself considered, but also the cabling, the appropriate connectors and the interfaces, and all associated expenses have to be considered as well [4]. Besides, the encoder also reduces the system reliability since it is susceptible to harsh environment. Therefore, various sensorless

control algorithms for the elimination of speed and position sensors have been proposed.

The sensorless control techniques for rotor position estimation are mainly classified into two categories: high-frequency injection (HFI) based methods and model-based methods. For zero- and low-speed motor operation, the HFI-based technique is used, however, it is prone to generating high-frequency noise, which affects system performance. Moreover, the accuracy of the position estimation depends strictly on the rotor saliency. A detailed discussion of feasibility region of HFI-based sensorless control methods for PMSMs can be found in [5].

The model-based sensorless control strategy is noninvasive and applicable for medium- and high-speed motor operations. For the model-based position sensorless control method of PMSMs, the extended electromotive force (EEMF) model [6] and the active flux (AF) model [7] (also defined as “extended rotor flux” model in [8] or “equivalent EMF” model in [9]) are the most popular models for PMSMs to obtain the related position information. Both of these two models have their own benefits and limitations. For the EEMF model, its magnitude varies with the motor speed. At low-speed conditions, its magnitude is very difficult to accurately extract due to the small signal-to-noise ratio (SNR). Compared to the EEMF model, a salient feature of the AF model is its constant magnitude regardless of rotating speed. However, an integrator is normally required to calculate the flux terms. In this case, some practical issues, e.g., current sensor dc offset, integrator dc offset, and initial condition, should be carefully handled [10]. In order to simplify the paper representation, the EEMF model is used in the equations and figures of the article and the AF model for PMSMs is provided in Appendix A.

Various model-based position observers have been proposed to extract position information from EEMF model or AF model, such as the linear observer method [11], [12], [13], [14], sliding mode observer (SMO) method [1], [2], [15], and Kalman filter (KF) method [16], [17], [18], [19]. For linear observers, such as the Luenberger observer, the main advantage is its simple structure. However, as a nonlinear and strong coupling system, the characteristic of the PMSM cannot be well estimated by linear observers, which may result in poor estimation performance and even instability in the sensorless control system. Additionally, for linear observers, the gain design is based on the pole placement technique and system uncertainty and external noise are not taken into account. In contrast, the KF-based methods, such as the extended Kalman filter [19], compute the observer gain matrix in each controlling cycle to balance trust

Manuscript received 19 December 2022; revised 22 March 2023; accepted 3 June 2023. Date of publication 20 June 2023; date of current version 28 July 2023. This work was supported in part by the Natural Sciences and Engineering Research Council of Canada and Magna International Inc. Recommended for publication by Associate Editor T. Shi. (*Corresponding author: Chunyan Lai.*)

Ying Zuo and Chunyan Lai are with the Department of Electrical and Computer Engineering, Concordia University, Montreal, QC H3G 1M8, Canada. (e-mail: ying.zuo@concordia.ca; chunyan.lai@concordia.ca).

K. Lakshmi Varaha Iyer is with the Corporate Engineering and R&D, Magna International Inc., Troy, MI 48098 USA. (e-mail: lakshmivaraha.iyer@ieee.org).

Color versions of one or more figures in this article are available at <https://doi.org/10.1109/TPEL.2023.3287828>.

Digital Object Identifier 10.1109/TPEL.2023.3287828

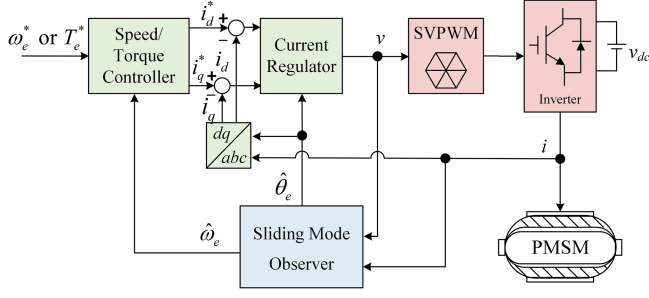


Fig. 1. Block diagram of SMO-based sensorless control of PMSM.

between model and sensor accuracy. Therefore, good robustness and anti-disturbance ability can be achieved. However, the high computational cost and difficulty in designing the covariance matrices cannot be ignored in the real implementation. Nowadays, the SMO approach has become one of the most popular position sensorless control methods for PMSMs due to its robustness and straightforward implementation. As a nonlinear observer, the control loop in the traditional linear observer is replaced by a sliding-mode variable structure in the SMO. Therefore, there are only two operating states of the system (e.g., “ON”/“OFF” or “forward”/“reverse”). These two operating states are artificially set, so they only depend on the selected convergence variables and are insensitive to parameter variations that enter into the sliding mode control channel [20], [21], [22]. Overall, the SMO approach is robust while having a simple structure. These favorable properties make SMO the mainstream model-based position sensorless control method for industrial applications.

This article aims to present a comprehensive review of the state-of-the-art solutions for SMO-based position sensorless control of PMSM drives. First, the design of SMO for position sensorless control of PMSMs in two different reference frames (stationary coordinate and estimated rotating coordinate), is systematically studied. Then, the relevant contributions recently reported in the literature to overcome the main technical limitations for SMO used in position sensorless control for PMSMs, including the chattering phenomenon and infinite-time convergence, are analyzed and summarized. The nonideal effects of parameter variation, low-frequency ratio, and inverter nonlinearity on the SMO-based position sensorless control are also investigated. Finally, the existing challenges and future trends are discussed.

## II. REVIEW OF EXISTING SMO-BASED SENSORLESS CONTROL

Fig. 1 represents the block diagram of the PMSM sensorless control system with the conventional SMO. Instead of the mechanical position sensor, the SMO is used to estimate the position and speed of the rotor by using the stator voltage and current measurements. Then, the estimated position and speed can be used for speed control and coordinate transformation. The design of SMO for PMSM position sensorless control system can be carried out in two different reference frames: stationary  $\alpha\beta$  coordinate and estimated rotating  $dq$  coordinate ( $d^v$ - $q^v$  axis), as shown in Fig. 2. In this section, the design of SMO is reviewed along with comparisons in two different coordinate systems.

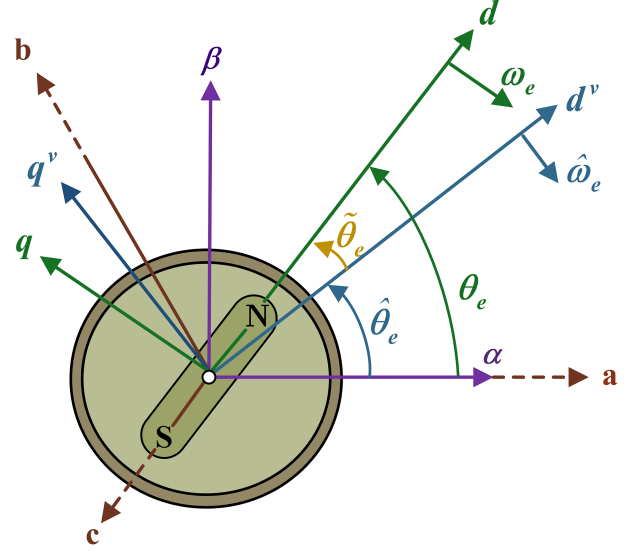


Fig. 2. Different reference frames in a PMSM drive.

### A. SMO Design in Stationary $\alpha\beta$ Coordinate System

The EEMF model of a PMSM in the stationary coordinate system can be represented as

$$\begin{cases} \mathbf{u}_{\alpha\beta} = \begin{bmatrix} R_s & -\omega_e L_\Delta \\ \omega_e L_\Delta & R_s \end{bmatrix} \mathbf{i}_{\alpha\beta} + \begin{bmatrix} L_d & 0 \\ 0 & L_d \end{bmatrix} \frac{d\mathbf{i}_{\alpha\beta}}{dt} + \mathbf{e}_{\alpha\beta} \\ \mathbf{e}_{\alpha\beta} = E_{ex} \begin{bmatrix} -\sin \theta_e \\ \cos \theta_e \end{bmatrix} \\ E_{ex} = (L_d - L_q) \left( \omega_e i_d - \frac{di_q}{dt} \right) + \omega_e \psi_f \end{cases} \quad (1)$$

where  $E_{ex}$  represents the EEMF, which was first introduced in [6];  $\mathbf{u}_{\alpha\beta} = [u_\alpha \ u_\beta]^T$  and  $\mathbf{i}_{\alpha\beta} = [i_\alpha \ i_\beta]^T$  are the stator voltage and current vectors in the  $\alpha\beta$  axis, respectively;  $\mathbf{e}_{\alpha\beta} = [e_\alpha \ e_\beta]^T$  is the EEMF in the  $\alpha\beta$  axis;  $R_s$  is the stator resistance of PMSM;  $L_d$  and  $L_q$  are the  $d$ - $q$  axis inductances of PMSM;  $\omega_e$  is the rotor electric angular speed;  $\theta_e$  is the electrical angle of the rotor;  $\psi_f$  is the permanent magnet flux;  $i_d$  and  $i_q$  are stator currents in the  $d$ - $q$  axis, respectively; and  $L_\Delta = L_q - L_d$ .

The EEMF contains the information of the rotor position and speed of the motor. Therefore, the speed and position information of the motor can be calculated from the EEMF. Taking  $\alpha\beta$  axis currents as the state variables, (1) can be transformed into the state equation of the stator currents as follows:

$$\frac{d\mathbf{i}_{\alpha\beta}}{dt} = \begin{bmatrix} -\frac{R_s}{L_d} & \frac{\omega_e L_\Delta}{L_d} \\ -\frac{\omega_e L_\Delta}{L_d} & -\frac{R_s}{L_d} \end{bmatrix} \mathbf{i}_{\alpha\beta} + \frac{1}{L_d} (\mathbf{u}_{\alpha\beta} - \mathbf{e}_{\alpha\beta}). \quad (2)$$

To obtain the estimated EEMF, the conventional SMO in the  $\alpha\beta$  axis is designed as

$$\frac{d\hat{\mathbf{i}}_{\alpha\beta}}{dt} = \begin{bmatrix} -\frac{R_s}{L_d} & \frac{\hat{\omega}_e L_\Delta}{L_d} \\ -\frac{\hat{\omega}_e L_\Delta}{L_d} & -\frac{R_s}{L_d} \end{bmatrix} \hat{\mathbf{i}}_{\alpha\beta} + \frac{1}{L_d} (\mathbf{u}_{\alpha\beta} - \mathbf{z}_{\alpha\beta}) \quad (3)$$

where  $\mathbf{z}_{\alpha\beta} = [z_\alpha \ z_\beta]^T$  is the control input of the observer; and the symbol “ $\hat{\cdot}$ ” represents the estimated value.

Since the stator current is the only physical quantity that can be measured, the sliding surface is selected on the stator current

path as

$$\mathbf{s}_{\alpha\beta} = \tilde{\mathbf{i}}_{\alpha\beta} = \hat{\mathbf{i}}_{\alpha\beta} - \mathbf{i}_{\alpha\beta} \quad (4)$$

where the symbol “ $\sim$ ” represents the variable error, which refers to the difference between the observed value and the actual value. Then, the sliding mode control law is defined as

$$\mathbf{z}_{\alpha\beta} = \mathbf{K}_{\alpha\beta} \text{sgn}(\tilde{\mathbf{i}}_{\alpha\beta}) \quad (5)$$

where  $\text{sgn}(x)$  is the sign function and  $\mathbf{K}_{\alpha\beta} = [K_\alpha \ K_\beta]$  is the sliding mode gain in the  $\alpha$ - $\beta$  axis.

Taking (2) and (3) as the difference, the error equation of stator currents can be obtained as

$$\begin{cases} \frac{d\tilde{i}_\alpha}{dt} = -\frac{R_s}{L_d}\tilde{i}_\alpha - \frac{L_\Delta}{L_d}(\hat{\omega}_e\hat{i}_\beta - \omega_e i_\beta) + \frac{1}{L_d}(e_\alpha - z_\alpha) \\ \frac{d\tilde{i}_\beta}{dt} = -\frac{R_s}{L_d}\tilde{i}_\beta + \frac{L_\Delta}{L_d}(\hat{\omega}_e\hat{i}_\alpha - \omega_e i_\alpha) + \frac{1}{L_d}(e_\beta - z_\beta) \end{cases} \quad (6)$$

In order to analyze the stability of SMO, make the positive definite function be a Lyapunov function's candidate

$$\mathbf{V}_{\alpha\beta} = \frac{1}{2}\mathbf{s}_{\alpha\beta}^T \mathbf{s}_{\alpha\beta} = \frac{1}{2}(s_\alpha^2 + s_\beta^2). \quad (7)$$

According to the Lyapunov stability theorem, when the Lyapunov equation satisfies  $dV/dt < 0$  for  $V > 0$ , the system is asymptotically stable [1]. Taking the derivative of (7), following equation can be obtained:

$$\frac{d\mathbf{V}_{\alpha\beta}}{dt} = \left( s_\alpha \frac{ds_\alpha}{dt} + s_\beta \frac{ds_\beta}{dt} \right). \quad (8)$$

Based on (7), it is clear that  $\mathbf{V}_{\alpha\beta} > 0$ . Then, according to the Lyapunov stability theorem, by deducing  $d\mathbf{V}_{\alpha\beta}/dt < 0$ , we can conclude that the SMO can reach a stable state. Substituting (4) into (8),  $d\mathbf{V}_{\alpha\beta}/dt$  can be derived as

$$\begin{aligned} & \frac{d\mathbf{V}_{\alpha\beta}}{dt} \\ &= \tilde{i}_\alpha \cdot \frac{d\tilde{i}_\alpha}{dt} + \tilde{i}_\beta \cdot \frac{d\tilde{i}_\beta}{dt} \\ &= \tilde{i}_\alpha \left( -\frac{R_s}{L_d}\tilde{i}_\alpha - \frac{L_\Delta}{L_d}(\hat{\omega}_e\hat{i}_\beta - \omega_e i_\beta) + \frac{1}{L_d}(e_\alpha - z_\alpha) \right) \\ & \quad + \tilde{i}_\beta \left( -\frac{R_s}{L_d}\tilde{i}_\beta + \frac{L_\Delta}{L_d}(\hat{\omega}_e\hat{i}_\alpha - \omega_e i_\alpha) + \frac{1}{L_d}(e_\beta - z_\beta) \right). \end{aligned} \quad (9)$$

To satisfy  $d\mathbf{V}_{\alpha\beta}/dt < 0$ , (9) is decomposed into two equations as

$$\begin{cases} -\frac{R_s}{L_d}(\tilde{i}_\alpha^2 + \tilde{i}_\beta^2) < 0 \\ \frac{\tilde{i}_\alpha}{L_d}(e_\alpha - K_\alpha \text{sgn}(\tilde{i}_\alpha)) + \frac{\tilde{i}_\beta}{L_d}(e_\beta - K_\beta \text{sgn}(\tilde{i}_\beta)) < 0. \end{cases} \quad (10)$$

Therefore, the observer gain matrix  $\mathbf{K}_{\alpha\beta}$  can be derived to satisfy the inequality condition as

$$\mathbf{K}_{\alpha\beta} > \max(|e_{\alpha\beta}|). \quad (11)$$

Based on the above analysis, when the gain  $\mathbf{K}_{\alpha\beta}$  satisfies the condition in (11), the system state will reach the sliding surface. When the state variable of the observer reaches the

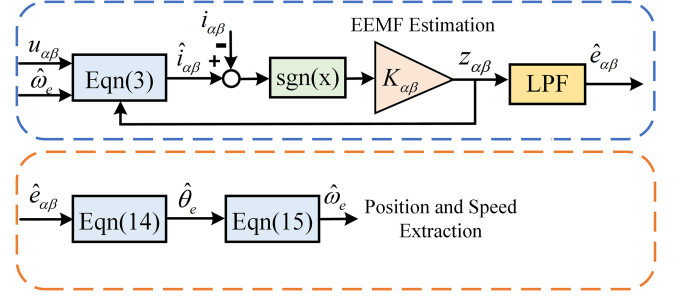


Fig. 3. Block diagram of the conventional SMO design in stationary  $\alpha\beta$  coordinate system.

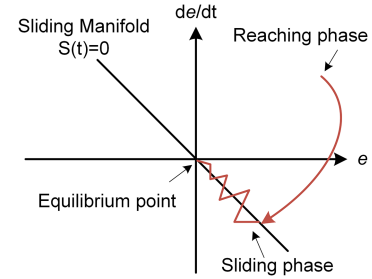


Fig. 4. Graphical representation of sliding mode control [27].

sliding surface  $s = 0$ , the observer state will always remain on the sliding surface. When the system reaches the sliding surface, the following equation can be obtained based on (2) and (3):

$$\mathbf{e}_{\alpha\beta} = \mathbf{z}_{\alpha\beta} = \mathbf{K}_{\alpha\beta} \text{sgn}(\tilde{\mathbf{i}}_{\alpha\beta}) \quad (12)$$

which means that the EEMF can be estimated by using the equivalent control of the observer. Based on (12), the actual control signals are discontinuous switching signals. Therefore, a low-pass filter (LPF) is normally used to extract EEMF components as

$$\hat{\mathbf{e}}_{\alpha\beta} = \frac{\omega_{\text{cutoff}}}{s + \omega_{\text{cutoff}}} \mathbf{z}_{\alpha\beta} \quad (13)$$

where  $\omega_{\text{cutoff}}$  represents the cutoff frequency of LPF. Then, the rotor position and speed can be estimated through the estimated EEMF based on (14) and (15). The overall block diagram for the conventional SMO in the  $\alpha$ - $\beta$  axis is presented in Fig. 3

$$\hat{\theta}_e = -\arctan\left(\frac{\hat{e}_\alpha}{\hat{e}_\beta}\right) \quad (14)$$

$$\hat{\omega}_e = \frac{d\hat{\theta}_e}{dt}. \quad (15)$$

However, due to the use of the arctangent function in (14), the estimated position and speed are sensitive to noise and harmonics. Serious estimation errors can be obtained when  $\hat{e}_\beta$  crosses zero if the arctangent function is used to extract the position information. Therefore, the phase-locked loop (PLL) algorithm is commonly used for position and speed extraction. However, it is noted that a rotor position error of  $180^\circ$  will be generated with conventional PLL when the speed direction is changed

[23], [24], [25]. Therefore, when both positive and negative speed of the PMSM is required, improved PLL algorithms, such as tangent function based PLL [23], can be used to guarantee position estimation accuracy.

### B. SMO Design in Rotating Estimated dq Coordinate System

The PMSM mathematical model in the rotating dq coordinate system based on EEMF model is given by

$$\begin{cases} \mathbf{u}_{dq} = \begin{bmatrix} R_s & -\omega_e L_q \\ \omega_e L_q & R_s \end{bmatrix} \mathbf{i}_{dq} + \begin{bmatrix} L_d & 0 \\ 0 & L_d \end{bmatrix} \frac{d\mathbf{i}_{dq}}{dt} + \mathbf{e}_{dq} \\ \mathbf{e}_{dq} = \begin{bmatrix} 0 \\ E_{ex} \end{bmatrix} \end{cases} \quad (16)$$

where  $\mathbf{u}_{dq} = [u_d \ u_q]^T$  and  $\mathbf{i}_{dq} = [i_d \ i_q]^T$  are the stator voltage and current vectors in the  $d$ - $q$  axis, respectively;  $\mathbf{e}_{dq} = [e_d \ e_q]^T$  is the EEMF components in the  $d$ - $q$  axis.

In the position sensorless control, the dq model cannot be directly utilized since the rotor position is not measured. Therefore, the mathematical model in the estimated dq coordinate system ( $d^v$ - $q^v$  axis), which lags by  $\theta_{vilde}$  from the real dq coordinate frame as shown in Fig. 2, is derived as follows by transforming (1) into the  $d^v$ - $q^v$  axis:

$$\begin{cases} \mathbf{u}_{d^v q^v} = \begin{bmatrix} R_s & -\omega_e L_{q^v} \\ \omega_e L_{q^v} & R_s \end{bmatrix} \mathbf{i}_{d^v q^v} + \begin{bmatrix} L_{d^v} & 0 \\ 0 & L_{d^v} \end{bmatrix} \frac{d\mathbf{i}_{d^v q^v}}{dt} + \mathbf{e}_{d^v q^v} \\ \mathbf{e}_{d^v q^v} = E_{ex} \begin{bmatrix} -\sin(\tilde{\theta}_e) \\ \cos(\tilde{\theta}_e) \end{bmatrix} + (\hat{\omega}_e - \omega_e) L_{q^v} \begin{bmatrix} -i_{q^v} \\ i_{d^v} \end{bmatrix} \end{cases} \quad (17)$$

where  $\mathbf{u}_{d^v q^v} = [u_{d^v} \ u_{q^v}]^T$  and  $\mathbf{i}_{d^v q^v} = [i_{d^v} \ i_{q^v}]^T$  are the stator voltage and current vectors in the  $d^v$ - $q^v$  axis, respectively;  $\mathbf{e}_{d^v q^v} = [e_{d^v} \ e_{q^v}]^T$  is the EEMF components in the  $d^v$ - $q^v$  axis; and  $L_{d^v}$  and  $L_{q^v}$  are the  $d^v$ - $q^v$  axis inductances. The design process of SMO in the  $d^v$ - $q^v$  axis is similar to the SMO design in the  $\alpha$ - $\beta$  axis and can be found in [26]. Due to the high-frequency switching function, the SMO designed in the  $\alpha$ - $\beta$  axis normally needs an LPF to extract EEMF components. However, it will inevitably introduce phase delay in the estimated position. On the other hand, the observed value is a dc signal for SMO designed in the  $d^v$ - $q^v$  axis, and the phase compensation is not required due to negligible delay. However, based on (17), when there is an error between real speed and estimated speed, the position error will exist even though  $d^v$ -axis EEMF  $e_{d^v}^v$  is controlled as zero. This position error will become more serious during the transient operation, where the estimated speed cannot perfectly track the real speed.

## III. REVIEW OF ENHANCED SMO DESIGN IN POSITION SENSORLESS CONTROL OF PMSMS

Although SMO is well-known for position sensorless control due to its easy implementation and robustness, two inherent problems, namely, chattering phenomenon generated by the discontinuous control law and infinite-time convergence caused by the linear sliding-mode surface, restrict the wide application of SMO. In this section, these technical problems of SMO are discussed, and various enhanced SMO-based position sensorless

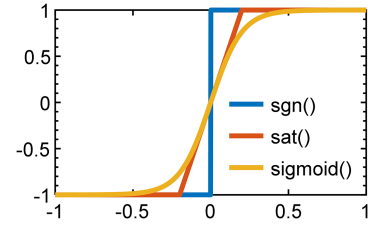


Fig. 5. Comparison of different switching function.

control strategies toward solving these inherent problems of SMO-based position sensorless control of PMSMs are reviewed.

### A. Enhanced SMO Toward Chattering Problem

Sliding mode control consists of two phases: reaching phase and sliding phase as shown in Fig. 4, in which  $e$  and  $de/dt$  denote the tracking error and first-order time derivative of the tracking error, respectively; and “ $t$ ” in  $s(t)$  is the independent time variable [27]. The basic principle of sliding mode control theory can be found in [28]. The main strength of using the  $\text{sgn}(x)$  function is its robustness, and the control action can be as simple as switching between two states: ON and OFF. It does not need to be very precise. Furthermore, it is not sensitive to parameter variations that enter into the control channel. However, the switching function  $\text{sgn}(x)$  causes the control gain to switch from one state to another every time the trajectory crosses the sliding manifold. Although in theory the trajectory is supposed to “slide” on the sliding manifold, in practice there are imperfections and delays in the switching devices, which leads to chattering [29]. And the chattering phenomenon will be aggravated with the high gain value set in the SMO. Therefore, unavoidable chatters may exist in the estimated position for the practical application. To deal with the chattering issue, different methods have been proposed in recent years as categorized as follows.

1) *Use of Smoother Switching Functions:* Many continuous switching functions have been proposed in state-of-the-art research work to replace the discontinuous  $\text{sgn}(x)$  function in the vicinity of sliding manifold to eliminate the chattering, such as the saturation function and the sigmoid function as shown in Fig. 5 [30], [31], [32], [33]. Inside the boundary layer, the switching function is approximated by a linear feedback gain instead of the discontinuous function. Based on the comparison study conducted in [34], the sigmoid function shows better performance for canceling the chattering problem compared to the other two switching functions. However, the boundary layer thickness has the tradeoff relation between control performance of sliding controller and chattering decrement [35]. Narrow boundary layer range increases convergence speed of the sliding mode motion but introduces chatters and harmonic distortions in EEMF estimations; while wide boundary range suppresses chatters but reduces robustness of the control system due to the approaching speed reduction and accumulates estimation errors due to the small gains near the switching boundary [36]. Therefore, using a constant high gain is insufficient to guarantee the performance of SMO-based sensorless control under all the operation conditions.



2) *Design of Higher Order SMO*: In [37], [38], and [39], the second-order (full-order) SMO is constructed by taking both current and EEMF as the state variables. In this way, the sliding mode gain only needs to be set higher than the maximum estimation error of EEMF, which means that the sliding mode gain is smaller and the chattering can be reduced

$$\frac{d}{dt} \begin{bmatrix} \hat{i}_{\alpha\beta} \\ \hat{e}_{\alpha\beta} \end{bmatrix} = \mathbf{A}_{\text{sec}} \begin{bmatrix} \hat{i}_{\alpha\beta} \\ \hat{e}_{\alpha\beta} \end{bmatrix} + \mathbf{B}_{\text{sec}} \mathbf{u}_{\alpha\beta} - \frac{\mathbf{K}_{\text{sec}}}{L_d} \text{sgn}(\hat{i}_{\alpha\beta} - i_{\alpha\beta}) \quad (18)$$

with

$$\mathbf{A}_{\text{sec}} = \begin{bmatrix} -\frac{R_s}{L_d} & \frac{\hat{\omega}_e L_d}{L_d} & -\frac{1}{L_d} & 0 \\ -\frac{\hat{\omega}_e L_d}{L_d} & -\frac{R_s}{L_d} & 0 & -\frac{1}{L_d} \\ 0 & 0 & 0 & -\hat{\omega}_e \\ 0 & 0 & \hat{\omega}_e & 0 \end{bmatrix};$$

$$\mathbf{B}_{\text{sec}} = \begin{bmatrix} \frac{1}{L_d} & 0 \\ 0 & \frac{1}{L_d} \\ 0 & 0 \\ 0 & 0 \end{bmatrix};$$

$$\mathbf{K}_{\text{sec}} = \begin{bmatrix} l_1 & 0 & m_1 & 0 \\ 0 & l_2 & 0 & m_2 \end{bmatrix}^T$$

where  $l_{1,2}$  and  $m_{1,2}$  are the gains. To ensure the stability of full-order SMO, the gains  $l_{1,2}$  need to satisfy [37]

$$l_{1,2} > \max(|\tilde{e}_{\alpha\beta}|). \quad (19)$$

Based on (19), the sliding mode gain only needs to be set higher than the maximum estimation error of EEMF. Although the second-order SMO can reduce the sliding mode gain by taking both currents and EEMFs as the state variables, its dynamic performance is limited since the derivatives of the EEMF terms are assumed zero and  $\text{sgn}(x)$  function is still adopted. Moreover, the computation burden is increased.

Another method to solve the chattering issue is to apply super-twisting algorithm (STA), which is also one of the second-order sliding mode algorithms, into the SMO-based sensorless control [40], [41], [42], [43], [44]. The sliding mode law in the STA-SMO is defined as

$$\begin{cases} z_{\text{STA}} = -k_{\text{STA},1} |\hat{i}_{\alpha\beta} - i_{\alpha\beta}|^{\frac{1}{2}} \text{sgn}(\hat{i}_{\alpha\beta} - i_{\alpha\beta}) + \xi_{\text{STA}} \\ \frac{d\xi_{\text{STA}}}{dt} = -k_{\text{STA},2} \text{sgn}(\hat{i}_{\alpha\beta} - i_{\alpha\beta}) \end{cases} \quad (20)$$

where  $z_{\text{STA}}$  is the control input of the STA-SMO;  $k_{\text{STA},1}$  and  $k_{\text{STA},2}$  are, respectively, the gains of the primary and auxiliary sliding surfaces. The selection rules of switching gains can be found in [44]. In the STA-SMO, as can be seen from (20), the high gain switching functions are transferred into the derivation of  $\xi_{\text{STA}}$  and then are added to  $z_{\text{STA}}$  through the integral, which is kind of equivalent to LPF of the high gain switching function and can essentially suppress the chattering. Therefore, STA has offered a method of enforcing sliding modes with continuous control action and as a result reducing chattering effect, caused by discontinuous input. However, the performance

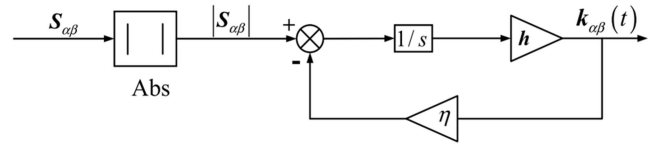


Fig. 6. Adaptive control algorithm for SMO [53].

of STA-SMO is sensitive to the selection rules of switching gains:  $k_{\text{STA},1}$  and  $k_{\text{STA},2}$  [45], [46], [47], [48], [49], and there is always a tradeoff for the gain selection in STA-SMO. Therefore, several adaptive observers have been proposed online tuning of the sliding mode gains based on perturbation in [50] and [51].

3) *Use of an Adaptive Gain*: The reason to use constant high gain is due to the upper bound of unknown disturbances. To reduce the chattering caused by the constant high gain, different adaptive SMO design methods have been proposed in recent years. For example, the upper bound of EEMF can be directly calculated based on the machine parameters and operating points in [52]. However, the accuracy of this method has a strong parameter dependence. Without the knowledge of uncertainties bound, the adaptive control algorithm concept is introduced in the adaptive SMO design for position sensorless control of PMSMs to reduce chattering in [53]. The adaptive gain algorithm is defined as follows and shown in Fig. 6:

$$\mathbf{K}_{\alpha\beta}(t) = h \int_{t_0}^t (|s_{\alpha\beta}| - \eta \mathbf{K}_{\alpha\beta}(t)) dt \quad (21)$$

where  $h$  and  $\eta$  are positive constants. When  $|s_{\alpha\beta}| > \eta \mathbf{K}_{\alpha\beta}$ , the switching gain  $\mathbf{K}_{\alpha\beta}$  increases until  $|s_{\alpha\beta}| \leq \eta \mathbf{K}_{\alpha\beta}$ . As the switching gain  $\mathbf{K}_{\alpha\beta}$  becomes larger, the sliding variable  $s_{\alpha\beta}$  will tend to approach the sliding manifold more quickly. Once  $|s_{\alpha\beta}| = 0$ , the adaptive gain will stop increasing and become a constant value that satisfies the reaching condition. Once the sliding mode is destroyed when speed or load torque changes, the adaptive gain will change with respect to the current perturbations until the sliding mode starts again. This method can ensure the existence and stability of the adaptive sliding motion without the knowledge of uncertainties bound. However, the selection of  $h$  and  $\eta$  still needs the prior knowledge.

In [54], [55], and [56], fuzzy logic control theory is employed to adjust the high constant gain adaptively in the SMO to suppress the chattering phenomenon significantly without decreasing system stability. In this method, the conventional SMO structure is unchanged and a fuzzy logic controller (FLC) is designed and embedded into the SMO to change the observer gain adaptively with the output current error, which is a proportional factor of the observer gain. However, the FLC is designed with fixed universes based on experts' experience [54]. In order to increase the precision of control, more fuzzy control rules need to be designed. However, it will increase the difficulty of the design procedure and lead to the so-called rules explosion problem. Therefore, the existing fuzzy-logic-based SMO could be inefficient or not practical since it employs numerous design parameters and complex rules.

4) *Elimination of Reaching Phase*: As aforementioned, the discontinuous control ensures that the switching function

remains on the sliding manifold in spite of the uncertainties during the sliding phase. Since the robustness is not guaranteed during the reaching phase in the conventional SMO, the integral sliding mode observer (ISMO) is designed to eliminate the reaching phase by enforcing the sliding phase throughout the entire system response [57], [58]. Compared with the conventional SMO, the ISMO guarantees the sliding mode invariance from the beginning, and it realizes the chattering alleviation while ensuring a fast and accurate tracking [59], [60]. The ISMO control law consists of continuous nominal control and discontinuous control. The integral sliding surface for ISMO is designed as

$$s_{\alpha\beta} = (\hat{i}_{\alpha\beta} - i_{\alpha\beta}) + \lambda \int (\hat{i}_{\alpha\beta} - i_{\alpha\beta}) dt \quad (22)$$

where  $\lambda$  is a positive constant.

The idea behind the ISMO is that a high-frequency switching gain is designed to force the states to achieve the integral sliding surface, and then the integral action in the sliding surface drives the states to the desired equilibrium in the presence of mismatched uncertainties [59]. In the ISMO, smaller maximum control gain is required since the value is usually bigger during the reaching phase. However, integral action, on the other hand, is well recognized to have some negative consequences on control systems, such as excessive overshoot and a long settling time.

### B. Enhanced SMO Toward Finite-Time Convergence

To analyze the convergence characteristic of estimated EEMF, the estimation error of  $e_{\alpha\beta}$  is represented as (33)

$$\begin{bmatrix} e_\alpha - \hat{e}_\alpha \\ e_\beta - \hat{e}_\beta \end{bmatrix} = L_d \left( \frac{d}{dt} (\hat{i}_{\alpha\beta} - i_{\alpha\beta}) - \mathbf{A}_{\alpha\beta} (\hat{i}_{\alpha\beta} - i_{\alpha\beta}) \right) \quad (23)$$

with

$$\mathbf{A}_{\alpha\beta} = \begin{bmatrix} -\frac{R_s}{L_d} & \frac{\hat{\omega}_e L_d}{L_d} \\ -\frac{\hat{\omega}_e L_d}{L_d} & -\frac{R_s}{L_d} \end{bmatrix}.$$

In the conventional SMO, the errors between the actual current and the estimated current can be forced to zero according to the sliding mode control law when system state reaches the sliding surface. However, the derivative of current errors cannot be guaranteed to zero. Therefore, based on (23), the estimated EEMF cannot achieve finite-time convergence to zero when the derivative of current errors is nonzero, which causes errors in the estimated rotor position. To solve this issue, the nonlinear surface is introduced in the design of SMO.

The concept of terminal sliding mode (TSM) was first proposed in [61] to guarantee a finite-time convergence of the states. The finite-time convergence in this article means that the sliding manifold can be reached in a finite time. However, the singularity problem exists with traditional TSM, which means, in some areas of the state space, the control input may require to be infinitely large in order to maintain the ideal TSM motion. Due to this singularity problem, TSM theory cannot be directly applied to SMO-based position observers in the practical application. To solve this issue, the nonsingular terminal sliding mode observer

(NTSMO) has been proposed in [62], [63], [64], and [65], which can provide a finite convergence time and avoid singularity at the same time. The nonlinear sliding surface for NTSMO is defined as

$$s_{\alpha\beta} = (\hat{i}_{\alpha\beta} - i_{\alpha\beta}) + \sigma \frac{d}{dt} (\hat{i}_{\alpha\beta} - i_{\alpha\beta})^{\frac{p_1}{q_1}} \quad (24)$$

where  $\sigma > 0$  and  $1 < (p_1/q_1) < 2$ . Based on [64], [65], [66], and [67], the NTSMO manifold (24) will be reached in a finite time. Suppose that  $t_r$  is the time when  $s_{\alpha\beta}$  reaches zero from  $s(0) \neq 0$ . Once the sliding surface  $s_{\alpha\beta}$  reaches zero, it will stay at zero. Based on (24), the errors between the actual current and the estimated current and their derivation will converge to zero within a finite time. The total convergence time  $t_s$  is given as

$$t_s = t_r + \frac{p_1}{p_1 - q_1} \max_{j=\alpha,\beta} \left( \frac{1}{\sigma} \left| \frac{q_1}{p_1} \right| \left| (\hat{i}_j - i_j) \right| (t_r) \right)^{\frac{p_1 - q_1}{p_1}}. \quad (25)$$

Although the nonlinear sliding manifold is used to ensure the finite-time convergence, the discontinuous switching function is embedded in first-order derivatives in the NTSMO. Therefore, it still suffers from chattering. To achieve the chattering suppression and the finite-time convergence simultaneously, the higher order terminal sliding mode (HOTSMO) method has been designed. The main idea of HOTSMO is to incorporate integral errors of states into the terminal sliding surface [68]. The sliding mode law in the HOTSMO is defined as

$$\begin{cases} z_{\alpha\beta\_HOTSMO} = -\beta \left| \hat{i}_{\alpha\beta} - i_{\alpha\beta} \right|^\gamma \text{sgn}(\hat{i}_{\alpha\beta} - i_{\alpha\beta}) + \xi_1 \\ \frac{d\xi_1}{dt} = -k_1 \text{sgn}(s_{TSMO}) + \omega_f \xi_1 \\ s_{TSMO} = \frac{d}{dt} (\hat{i}_{\alpha\beta} - i_{\alpha\beta}) + \beta (\hat{i}_{\alpha\beta} - i_{\alpha\beta})^\gamma \\ \text{sgn}(\hat{i}_{\alpha\beta} - i_{\alpha\beta}) \end{cases} \quad (26)$$

where  $k_1$ ,  $\xi_1$ ,  $\omega_f$ ,  $\beta$ , and  $\gamma$  are designed parameters.

The proof of stability and finite-time convergence can be found in [68] and [69]. Based on (26), the chattering suppression is achieved by transferring the discontinuous control into the derivatives of second-order control law and the convergence in finite time is achieved through the designed terminal sliding surface. Even though the HOTSMO can realize chattering suppression and finite-time convergence simultaneously, the practical design of HOTSMO is still a challenge. There are five unknown parameters in (26) that need to be selected, which undoubtedly brings difficulty to the observer design. Besides, due to the complicated algorithm in the HOTSMO, the computational time is long in the HOTSMO when implemented in the processor. Based on the results presented in [69], the computational time of the HOTSMO is around twice of the traditional SMO. To conclude this section, the state-of-the-art design of SMO for sensorless control of PMSM is summarized and compared in terms of their remarkable properties and disadvantages in Table I.

## IV. DESIGN OF SMO UNDER NONIDEAL CONDITIONS

In the ideal case, the control signal generated by the sliding mode control law is discontinuous and switches at infinity frequency with finite amplitude, which assures the sliding motion

TABLE I  
SUMMARY OF ENHANCED SMO DESIGNS FOR ADDRESSING INHERENT PROBLEMS IN THE CONVENTIONAL SMO

Inherent problems	Approaches	Type of SMO	Advantages	Disadvantages
Chattering	Use of smoother switching functions	Boundary layer SMO [30], [31] [31], [32], [33], [34], [35], [36]	<ul style="list-style-type: none"> <li>Replace the discontinuous function to smooth output</li> </ul>	<ul style="list-style-type: none"> <li>Sacrifice the system's robustness</li> <li>Steady-state error depending on boundary layer selection</li> </ul>
	Design of higher order SMO	Full-order SMO [37], [38], [39] STA-SMO [40], [41], [42], [43] [44], [50], [51]	<ul style="list-style-type: none"> <li>Smaller control gain required</li> <li>Satisfactorily attenuate chattering issue</li> </ul>	<ul style="list-style-type: none"> <li>Limited dynamic performance</li> <li>Performance is sensitive to parameter selection</li> </ul>
	Use of an adaptive gain	Adaptive SMO [52], [53]	<ul style="list-style-type: none"> <li>Without the knowledge of uncertainties bound</li> </ul>	<ul style="list-style-type: none"> <li>Stability is sensitive to parameter selection</li> </ul>
		FLC-SMO [54], [55], [56]	<ul style="list-style-type: none"> <li>Robustness with disturbance</li> </ul>	<ul style="list-style-type: none"> <li>Require expert knowledge</li> </ul>
	Elimination of reaching phase	ISMO [58], [59], [60]	<ul style="list-style-type: none"> <li>Fast and accurate tracking</li> <li>Smaller control gain required</li> </ul>	<ul style="list-style-type: none"> <li>Potential overshoot due to integral action</li> </ul>
Finite-time Convergence	Design of nonlinear sliding surface	NTSMO [62], [63], [64], [65], [66], [67]	<ul style="list-style-type: none"> <li>Fast convergence to the desired state</li> </ul>	<ul style="list-style-type: none"> <li>Chattering exists due to first order continuous control law</li> </ul>
		HOTSMO [69]	<ul style="list-style-type: none"> <li>Achieve chattering suppression and finite-time convergence simultaneously</li> </ul>	<ul style="list-style-type: none"> <li>Complicated tuning procedures</li> <li>Long computational time</li> </ul>

under disturbance and uncertainty [70]. However, such perfect performance can only be achieved in the ideal case. In the real implementation, the SMO performance will be degraded due to the physical limitations of switching, which leads to a change in control laws aimed at achieving an effective tradeoff between tracking performance and system uncertainty. To maintain the high performance of SMO-based sensorless control, the design of SMO under nonideal conditions is reviewed in this section.

#### A. Machine Parameter Variation

Accurate machine parameters, such as stator resistance and stator inductance, are required for high-performance SMO-based sensorless control. The change of machine parameters brings deviations to the estimated EEMF, thereby reducing the accuracy of the position estimation. The sensitivity analysis technique proposed in [71] is used here to investigate the steady-state parameter sensitivity for EEMF estimation. It is noted that the sensitivity analysis is carried out at steady state, where the sensitivity equations for both EEMF model and AF model are mathematically identical [71]. The sensitivity function of  $f$  with respect to a variable  $m$  is defined as the ratio between the relative variation of the function ( $df/f$ ) with respect to the relative parameter variation ( $dm/m$ ) is

$$S_m^f(x, m) = \frac{df}{dm} \frac{m}{f} = S_m^{|f|}(x, m) + j\phi S_m^\phi(x, m) \quad (27)$$

where  $|f|$  denotes the magnitude, and  $\phi$  is the phase. As the rotor position exists in the phase of the EEMF only, it can be deduced that the parameter mismatch will result in the position estimation error only if the sensitivity function is a complex number [72]. First, the sensitivity of the stator resistance is analyzed in the computation of the EEMF based on the sensitivity function as shown in (28). The derivation procedure is the same as [72]

$$S_{R_s}^{\text{EEMF}} = \frac{de_{\alpha\beta}}{dR_s} \frac{R_s}{e_{\alpha\beta}} = -\frac{R_s \dot{i}_{\alpha\beta}}{e_{\alpha\beta}} = \frac{R_s |I_s|}{E_{ex}} e^{j\theta'} \quad (28)$$

where  $I_s$  is the current magnitude.  $\theta'$  is the angle between the  $d$ -axis and the phase current, which represents the additional current phase to get a maximum torque-per-ampere control.

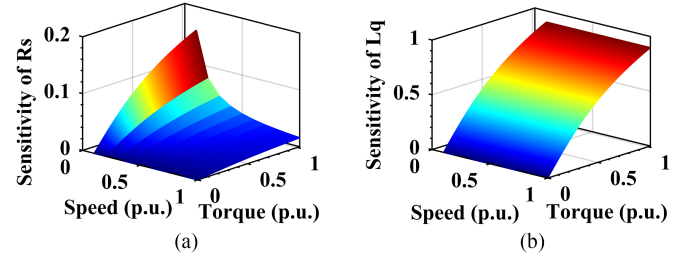


Fig. 7. Parameter sensitivity analysis of EEMF estimation. (a) Stator resistance. (b)  $q$ -axis inductance.

The sensitivity (28) results in a complex number. Therefore, the resistance mismatch reflects in a position estimation error, since the phase sensitivity is quantified by the imaginary part.

The sensitivity to the  $dq$ -axis inductances uncertainty is presented as

$$\begin{cases} S_{L_q}^{\text{EEMF}} = \frac{de_{\alpha\beta}}{dL_q} \frac{L_q}{e_{\alpha\beta}} = \frac{L_q \omega_e |I_s|}{E_{ex}} e^{j\theta'} \\ S_{L_d}^{\text{EEMF}} = \frac{de_{\alpha\beta}}{dL_d} \frac{L_d}{e_{\alpha\beta}} = \frac{L_d}{E_{ex}} \left| \frac{di_q}{dt} \right| \end{cases} \quad (29)$$

It can be seen from (29) that the  $q$ -axis inductance sensitivity function is a complex function, but that of the  $d$ -axis inductance is a real value. Therefore,  $d$ -axis inductance mismatch has no effects on EEMF-based position estimation. The parameter sensitivity analysis results are shown in Fig. 7. PMSM parameters are referred to [72].

As can be seen from Fig. 7, the stator resistance is essential in the low-speed range and  $q$ -axis inductance can lead to a dominant position estimation error for the EEMF estimation under the heavy load. Therefore, both stator resistance and  $q$ -axis inductance need to be identified accurately for EEMF-based SMO of position estimation, especially in the low-speed and high torque region.

Additionally, the variation of machine parameters would also change the convergence condition of the sliding-mode motion. Assuming that there are mismatches between machine real parameters and nominal parameters used in the SMO, (3) will be

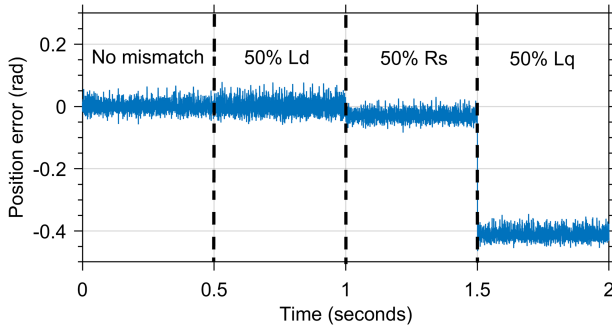


Fig. 8. Position error simulation results with SMO under different parameter mismatches conditions.

updated as

$$\frac{d\hat{\mathbf{i}}_{\alpha\beta}}{dt} = \mathbf{A}_{\alpha\beta}\hat{\mathbf{i}}_{\alpha\beta} + \frac{\mathbf{u}_{\alpha\beta}}{L_{d,n}} - \frac{\mathbf{z}_{\alpha\beta}}{L_{d,n}} + \Delta\mathbf{A}_{\alpha\beta}\hat{\mathbf{i}}_{\alpha\beta} \quad (30)$$

with

$$\Delta\mathbf{A}_{\alpha\beta} = \begin{bmatrix} -\frac{\Delta R_s}{L_{d,n}} & \frac{\hat{\omega}_e(\Delta L_q - \Delta L_d)}{L_{d,n}} \\ -\frac{\hat{\omega}_e(\Delta L_q - \Delta L_d)}{L_{d,n}} & -\frac{\Delta R_s}{L_{d,n}} \end{bmatrix}$$

where  $\Delta R_s$ ,  $\Delta L_d$ , and  $\Delta L_q$  are difference between nominal stator resistance,  $d$ -axis inductance, and  $q$ -axis inductance used in SMO and their actual values, respectively;  $L_{d,n} = L_d + \Delta L_d$  is nominal  $d$ -axis inductance. Taking (2) and (30) as the difference, the error equation of stator currents can be obtained as

$$\begin{aligned} \frac{d\tilde{\mathbf{i}}_{\alpha\beta}}{dt} &= \mathbf{A}_{\alpha\beta}\tilde{\mathbf{i}}_{\alpha\beta} + \frac{\mathbf{e}_{\alpha\beta} - \mathbf{z}_{\alpha\beta}}{L_d} \\ &+ \frac{L_{d,n}}{L_d}\Delta\mathbf{A}_{\alpha\beta}\hat{\mathbf{i}}_{\alpha\beta} - \frac{\Delta L_d}{L_d}\frac{d}{dt}\hat{\mathbf{i}}_{\alpha\beta}. \end{aligned} \quad (31)$$

Based on the Lyapunov stability theorem, the observer gain matrix  $\mathbf{K}_{\alpha\beta}$  can be derived as

$$\mathbf{K}_{\alpha\beta} > \max \left( |\mathbf{e}_{\alpha\beta}| + \Delta L_d \frac{d}{dt}\hat{\mathbf{i}}_{\alpha\beta} \right). \quad (32)$$

When the sliding mode gain satisfies (32), the sliding mode motion occurs and the estimated current error will converge to zero but with chattering caused by  $\Delta L_d$  [73]. Based on the above analysis, the resistance and  $q$ -axis inductance mismatches will directly reflect in a position estimation error, and  $d$ -axis inductance mismatch will introduce chattering in the estimated position. The simulation results for conventional SMO designed in (3) with different parameter variations are shown in Fig. 8 at 300 r/min and 20 Nm. PMSM parameters are referred to [72]. Consistent with the analysis results, both changes in resistance and  $q$ -axis inductance cause estimation errors, while  $d$ -axis inductance mismatch produces the chattering in the estimation error. Therefore, stator resistance and  $dq$ -axis inductance need to be identified accurately for EEMF-based SMO of position estimation.

The offline estimation of stator resistance is not sufficient because the actual value varies due to stator temperature. Several online resistance estimation methods for SMO-based sensorless control are proposed [74], [75], [77], [78], [79], [80],

[81], [82]. In [1], a first-order SMO with online resistor estimation is proposed. In [74], the MRAS-based resistance estimation method is proposed to further improve SMO performance. Using the estimated value of the variable stator resistance, the steady-state performance of SMO can be further improved. Due to magnetic saturation, stator inductances vary under different load conditions. The offline methods, such as finite-element method, can model the saturation effect fairly well, but the estimated values are often needed to be validated through experiments. Therefore, online inductance estimation is more suitable for a general-purpose motor drive. For example, the recursive least square method is used to identify the inductance parameters on the discrete-time model under SMO-based sensorless control [75], [76]. In [77], two adaptive schemes for inductance identification have been proposed considering magnetic saturation under sensorless control. The aforementioned methods can only estimate one machine parameter, by fixing other parameter to its nominal value to get a full-rank reference model under sensorless control and ignore the possible existing position error. However, when the stator resistance and inductances are not simultaneously estimated, the estimation of parameters will converge to the wrong values due to the mismatching of the other parameters that are fixed in the estimation [78]. To solve the rank-deficient problem for parameter identification under sensorless control, current/voltage injection is widely used to estimate multiple parameters for sensorless control, which can build a full-rank reference model [79], [80]. However, the signal injection based method will introduce noise to the drive system and also change the operation point. Advanced algorithms, such as affine projection algorithm (APA), are used for online multiparameter estimation [81], [82]. Under sensorless control, two APAs are employed to estimate the stator inductances and stator resistance separately. However, those advanced algorithms usually require a significant amount of convergence time and tuning the design parameters is not straightforward. Generally, the simultaneous identification of stator resistance and  $dq$ -axis inductance under position sensorless control is not much in the literature.

### B. Low-Frequency Ratio

Sliding mode requires high-frequency discontinuous action to steer the states of a system into a sliding surface and to maintain the subsequent motion on that surface [83]. However, due to the limited sampling frequency, control inputs are constant across two sampling periods, making it challenging to execute instantaneous actions in the discrete-time drive system. Therefore, it has been realized that directly applying SMO design in the continuous-time domain to discrete-time domain will lead to many problems, such as large chattering amplitude, sample/hold effects, discretization errors, or even instability [84], [85], [86], especially for high-speed application, when the frequency ratio of the pulsewidth modulation (PWM) frequency ( $f_{\text{PWM}}$ ) over the fundamental frequency ( $f_{\text{OUT}}$ ),  $f_{\text{ratio}} = f_{\text{PWM}}/f_{\text{OUT}}$ , is low. In the SMO, the inherent chattering and phase shift because of the sign function and LPF can influence EEMF waveforms and further lead to low estimation performance and accuracy. Under low-frequency ratio condition, the enlargement of control



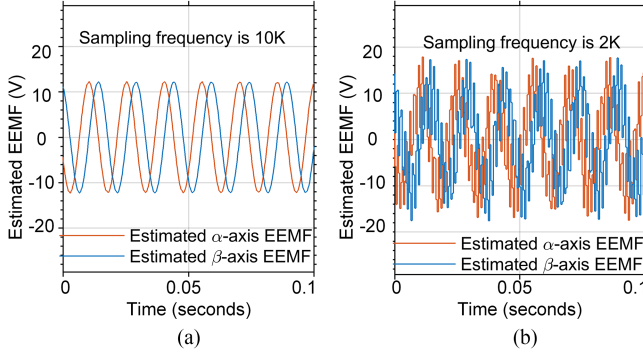


Fig. 9. Estimated EEMF waveforms under different sampling frequency. (a) 10 000 Hz. (b) 2000 Hz.

delay reduces the equivalent switching frequency of the sign function, which aggravates chattering of the SMO. Moreover, the fundamental frequency will be close to the switching frequency when the frequency ratio decreases, which deteriorates filtering effect of the LPF. These problems of the SMO-based position sensorless control under low-frequency ratio can be confirmed from the simulation results in Fig. 9. The estimated EEMF waveforms have more harmonics under low-frequency ratio.

In [86], quasi proportional-resonant (QPR) controller is employed in the SMO to extract the EEMF without the sliding mode switching function and LPF. Therefore, the chattering can be reduced under low-frequency ratio. However, as a nonlinear controller, careful analysis and design are usually required to ensure the performance of the QPR controller. Furthermore, the SMO design is still in the continuous-time domain, so the performance is only guaranteed when frequency ratio is higher than 15. To further improve the performance under low-frequency ratio, the discrete-time domain design is suggested. Different discrete-time SMO (DSMO) design methods have been proposed in recent years. The Euler approximation is commonly used for DSMO design, since it is simple and easy to implement [87], [88]. However, the traditional Euler approximation method may bring unwanted estimation errors and the SMO cannot work properly under low  $f_{ratio}$  condition. As reported in [89], the Euler-approximation-based SMO gets unstable when  $f_{ratio}$  is lower than 17.4. Therefore, Tustin approximation method is used in [90] for SMO-based sensorless control. The discrete-time domain SMO design in the stationary  $\alpha\beta$  coordinate system with Euler approximation and Tustin approximation discretization are given as follows:

$$\hat{i}_{\alpha\beta}(k+1) = \mathbf{A}_{Eul} \hat{i}_{\alpha\beta}(k) + \mathbf{B}_{Eul}(\mathbf{u}_{\alpha\beta}(k) - \hat{e}_{\alpha\beta}(k)) \quad (33)$$

with

$$\mathbf{A}_{Eul} = \begin{bmatrix} 1 - \frac{R_s T_s}{L_d} & \frac{T_s \omega_e (L_q - L_d)}{L_d} \\ -\frac{T_s \omega_e (L_q - L_d)}{L_d} & 1 - \frac{R_s T_s}{L_d} \end{bmatrix},$$

$$\mathbf{B}_{Eul} = \begin{bmatrix} \frac{T_s}{L_d} \\ \frac{T_s}{L_d} \end{bmatrix}^T$$

$$\hat{i}_{\alpha\beta}(k+1) = \mathbf{A}_{Tus} \hat{i}_{\alpha\beta}(k) + \mathbf{B}_{Tus}(\mathbf{u}_{\alpha\beta}(k) - \hat{e}_{\alpha\beta}(k)) \quad (34)$$

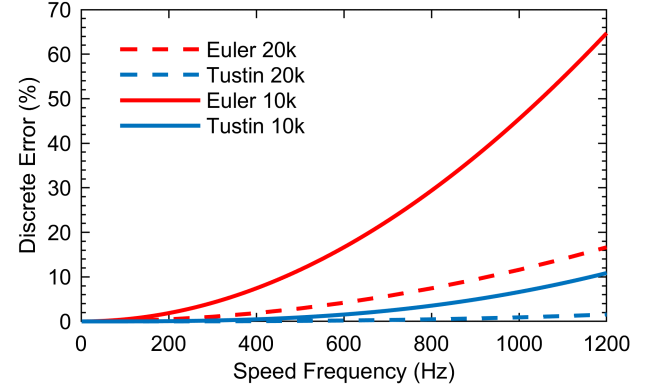


Fig. 10. Discretization error curves of different discretization methods.

with

$$\mathbf{A}_{Tus} = \frac{1}{d} \cdot \begin{bmatrix} 2b \left(1 - \frac{T_s R_s}{2L_d}\right) L_d - c^2 & -2c \left(1 - \frac{T_s R_s}{2L_d}\right) L_d - bc \\ 2c \left(1 - \frac{T_s R_s}{2L_d}\right) L_d + bc & 2b \left(1 - \frac{T_s R_s}{2L_d}\right) L_d - c^2 \end{bmatrix};$$

$$\mathbf{B}_{Tus} = \frac{\sqrt{T_s}}{d} \cdot \begin{bmatrix} 2b - 2c \\ 2b + 2c \end{bmatrix}^T;$$

$$b = T_s R_s + 2L_d; c = -T_s \omega_e L_d; d = c^2 + b^2$$

where  $T_s$  is the sampling time.

For the convenience of quantitative analysis, the matrix 2-norm is used to measure the discretization error [91]. Then, the discretization error of the DSMO for PMSMs can be expressed as

$$\text{err} = \left\| \frac{\Phi - e^{\mathbf{A}_{\alpha\beta} T_s}}{e^{\mathbf{A}_{\alpha\beta} T_s}} \right\|_2 \quad (35)$$

where  $\Phi$  is the state transition matrix.

By replacing  $\Phi$  in (35) with  $\mathbf{A}_{Eul}$  and  $\mathbf{A}_{Tus}$ , the discretization error of DSMO with Euler approximation and Tustin approximation can be calculated, respectively. In Fig. 10, discretization error curves as motor operating frequency increases (0–1200 Hz) for these two methods for DSMO design are compared at two different sampling frequencies (10 and 20 kHz). PMSM parameters are referred to [72]. As shown in Fig. 10, the discretization errors of Euler and Tustin approximation-based SMO grow with the increase of operating frequency and discrete step. However, the errors of Tustin-approximation-based SMO are significantly smaller than those of the Euler-approximation-based SMO for the same discrete step and operating frequency.

To further improve the precision, the Exact discretization method is introduced for DSMO design in [92], [93], and [94], which could achieve good performance with  $f_{ratio}$  down to 5. The discrete-time domain SMO design in the stationary  $\alpha\beta$  coordinate system with Exact discretization is given as

$$\hat{i}_{\alpha\beta}(k+1) = \mathbf{A}_{Exa} \hat{i}_{\alpha\beta}(k) + \mathbf{B}_{Exa}(\mathbf{u}_{\alpha\beta}(k) - \hat{e}_{\alpha\beta}(k)) \quad (36)$$

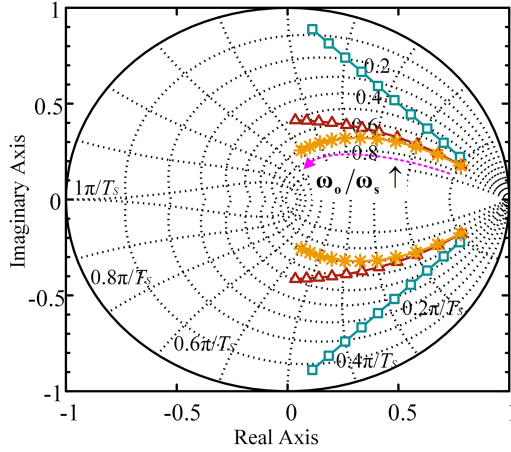


Fig. 11. Discrete-time pole migration comparison with  $\omega_0$  increase [93]. (□: Euler approximation; △: Tustin approximation; \*: Exact discretization).

with

$$\mathbf{A}_{\text{Exa}} = \begin{bmatrix} e^{-\frac{R_s T_s}{L_d}} \cos(X) (R_s^2 + \omega_e L_d) & -e^{-\frac{R_s T_s}{L_d}} \sin(X) (R_s^2 + \omega_e L_d) \\ e^{-\frac{R_s T_s}{L_d}} \sin(X) (R_s^2 + \omega_e L_d) & e^{-\frac{R_s T_s}{L_d}} \cos(X) (R_s^2 + \omega_e L_d) \end{bmatrix}$$

$$\mathbf{B}_{\text{Exa}} = \mathbf{A}_{\text{Exa}}^{-1} (e^{(\mathbf{A}_{\text{Exa}} T_s)} - \mathbf{I}); X = T_s \omega_e (1 - L_q / L_d)$$

where  $\mathbf{I}$  is the identity matrix, defined as  $\text{diag}(1, 1, 1, 1)$ .

The comparison of the pole migration for three different discretization method under speed changing is shown in Fig. 11, where  $\omega_0$  is the natural angular frequency of the observer and  $\omega_s = 2\pi/T_s$  is the sampling frequency. In Fig. 11, the observer poles move further to the left plane of the real axis with an increased  $\omega_0$ . It can be seen that both Exact discretization and Tustin approximation keep the system stable while the Euler discretization is highly oscillatory under high-speed region. However, compared to the Exact discretization method, Tustin approximation method cannot hold the constant damping factor for the whole speed range. The Exact discretization method can provide an exact discretized equivalent of the continuous-time plant for which discrete observer can be designed. However, there are too many trigonometric and exponential operations that need to be calculated. Therefore, the lookup tables for trigonometric and exponential operations are usually required for the real implementation with Exact discretization, which increases the memory usage.

### C. Inverter Nonlinearity

Voltage distortion, produced by voltage-source inverters (VSI), is caused by nonlinear characteristics of switching devices, such as dead time, turn-ON delay time, and turn-OFF delay time [95], [96], [97]. Although these times only account for a small portion of the PWM period, the VSI nonlinearity will become dominant in low-speed operation, resulting in mismatch between reference and actual voltage and  $(6k \pm 1)$ th harmonics in the  $\alpha$ - $\beta$  axis currents. These current harmonics will then introduce  $(6k \pm 1)$ th harmonics in the estimated EEMF. In

order to highlight the effect of harmonics, the estimated EEMF considering VSI nonlinearity can be defined as [97], [98], [99], [100]

$$\hat{\mathbf{e}}_{\alpha\beta} = \begin{bmatrix} e_{f\alpha} \\ e_{f\beta} \end{bmatrix} + \begin{bmatrix} e_{h\alpha} \\ e_{h\beta} \end{bmatrix} \quad (37)$$

with

$$\begin{bmatrix} e_{f\alpha} \\ e_{f\beta} \end{bmatrix} = \begin{bmatrix} -e_1 \sin(\omega_e t + \theta_{ei}) \\ e_1 \cos(\omega_e t + \theta_{ei}) \end{bmatrix}$$

$$\begin{bmatrix} e_{h\alpha} \\ e_{h\beta} \end{bmatrix} = \begin{bmatrix} -e_{6k\pm 1} \sin(\pm(6k \pm 1)\omega_e t + \theta_{e(6k\pm 1)}) \\ e_{6k\pm 1} \cos(\pm(6k \pm 1)\omega_e t + \theta_{e(6k\pm 1)}) \end{bmatrix}$$

where  $e_1$  and  $e_{6k\pm 1}$  represent the amplitude of fundamental and  $(6k \pm 1)$ th harmonic contents, respectively;  $\theta_{ei}$  and  $\theta_{e(6k\pm 1)}$  represent the corresponding initial phase angle. As a result, the estimated rotor position error is obtained as

$$\varepsilon_{\theta_e} = -(e_{f\alpha} + e_{h\alpha}) \cos \hat{\theta}_e - (e_{f\beta} + e_{h\beta}) \sin \hat{\theta}_e$$

$$= e_1 \sin(\theta_{ei} - \hat{\theta}_{ei}) + e_{6k} \sin(6k\omega_e t + \theta_{e(6k)}) \quad (38)$$

where  $e_{6k}$  represents the amplitude of the equivalent  $(6k)$ th EEMF harmonics and  $\theta_{e(6k)}$  represents the corresponding initial phase. Based on (38),  $(6k)$ th-order EEMF harmonics will display as additional errors which exist in the phase difference. As a result, the estimated rotor position will also contain the  $(6k)$ th-order harmonics.

In [101], [102], and [103], VSI nonlinearity compensation techniques have been widely discussed to remove harmonics in the estimated rotor position. However, these methods cannot be applied directly to SMO-based sensorless control due to the lack of position measurement. Therefore, several methods have been proposed for reducing the position estimation error caused by VSI nonlinearity in sensorless control, which can be classified into two categories: filters-based methods and feedforward-voltage-compensation-based methods [104]. For filter-based methods, different kinds of filter have been designed to reduce the estimated position error by filtering out the harmonics in estimated EEMF waveforms [98], [105], [106]. However, the performance depends on the accuracy of estimated motor frequency. Additionally, the mismatch between the reference voltage and the actual terminal voltage still exists in the drive. In feedforward-voltage-compensation-based methods, the compensated voltage is estimated based on minimizing the harmonics of the  $d$ -axis current or  $d$ -axis estimated back EMF [104], [107], [108], [109], [110]. However, the performance of voltage compensation methods depends on the accuracy of small-signal models of inverters. The summary of existing techniques for SMO design under nonideal conditions can be found in Table II.

### V. DISCUSSIONS AND FUTURE RESEARCH TRENDS

This article reviewed the state-of-the-art SMO-based position sensorless control of PMSMs. Due to its simple implementation and strong robustness, SMO for sensorless control has drawn much attention in recent years and opportunities of future work are still wide open. According to the literature, regardless of the well-known performance of conventional SMO in practical

TABLE II  
SUMMARY OF EXISTING TECHNIQUES FOR SMO DESIGN UNDER NONIDEAL CONDITIONS

Non-ideal condition	Effect on SMO performance	Existing techniques	Limitations on existing techniques
Parameter variation	▪ Offset and chattering in the estimated position	▪ MRAS [74], RLS [75], [76]	▪ Rank-deficient
		▪ Current/Voltage injection [79], [80]	▪ Introduce noise and change the operation point
Low-frequency ratio	▪ Offset and chattering in the estimated position ▪ Instability with increased speed	▪ Adaptive algorithms (e.g., APA[81], [82])	▪ Slow convergence and complex design
		▪ Resonant controller [86]	▪ Performance is sensitive to design parameters
Inverter nonlinearity	▪ Harmonics in the estimated position ▪ Limit the low-speed operation range	▪ Discrete-time design (e.g., Tustin approximation [90], Exact discretization [92], [93], [94])	▪ Computational burden
		▪ Advanced filtering [98], [105], [106]	▪ Performance is sensitive to the accuracy of estimated motor frequency
		▪ Feedforward voltage compensation [104], [107], [108], [109], [110]	▪ Require an accurate model of the inverter

applications, it still exhibits some weaknesses in delivering the desired performance when it comes to position sensorless control, especially when system uncertainties and external disturbances exist. The speed range and load capacity of SMO are also limited at the current stage.

Based on the observability analysis in [111], PMSM will lose observability of the rotor position as speed approaches zero and the signal injection technique is required to recover the observability of the motor. As reported in [112], the model-based sensorless control methods of PMSMs can only achieve satisfactory performance in medium- and high-speed regions (usually above 10% of the rated speed), and their performance deteriorates in zero- and very-low-speed regions due to the low SNR caused by harmonics and noise. As a model-based method, SMO performance also degrades in the low-speed region, especially at the presence of inverter nonlinearity. It has been shown in [99] that the position error can fluctuate up to 18° for conventional SMO with sign function without any inverter nonlinearity compensation when the rotor speed is 5% of rated speed and the VSI deadtime is 4  $\mu$ s. Therefore, SMO is mostly applied in medium- and high-speed operations. However, the SMO performance in the very-high-speed region also degrades due to chattering and the phase delay caused by the LPF. And when the sampling frequency is limited, the discretization methods can also show an impact on SMO performance in the high-speed operation. The load capacity for SMO-based sensorless control of PMSMs mainly depends on the  $dq$ -axis inductance variation levels of the motor. Based on the parameter analysis,  $q$ -axis inductance variation will introduce a constant offset in the estimation position error and  $d$ -axis inductance variation will introduce chattering the estimation position. Therefore, the identification of  $dq$ -axis inductance is important to increase the load capacity for SMO-based sensorless control of PMSMs.

The performances of position and speed estimation in SMO-based sensorless control is a critical factor in achieving optimal PMSM control performance and efficiency. As analysis conducted in [113] shows, position errors can introduce fundamental and second-order harmonic components in the motor output torque. Additionally, position errors can increase the required current amplitude and further reduce efficiency [114]. Therefore, it is essential to investigate high-performance SMO-based sensorless control strategies to achieve accurate position estimation and control, even in the presence of uncertainties and

disturbances. Toward these two main objectives of improving the position estimation accuracy and system stability, the potential future work of SMO-based PMSM sensorless control is discussed considering practical implementation and application requirements as follows, and it is outlined in Fig. 12.

#### A. Enhancement to SMO Inherent Limitations

Chattering is a primary factor that has a significant impact on the accuracy of SMO-based position sensorless control. Various chattering suppression techniques have been proposed to eliminate the chattering phenomenon as discussed in Section III-A. Although these methods have been validated through experiments, there are still important factors that should not be ignored during the design of SMO when adopting these chattering suppression techniques. First, when replacing the discontinuous function  $\text{sgn}(x)$  with a smoother continuous sliding surface in position sensorless control, there may exist the position estimation deviation. For instance, the deviation in position estimation caused by the use of sigmoid function has been analyzed and discussed in [115]. Therefore, it is important to take effective measures to compensate for the position estimation error caused by the continuous sliding surface. Second, when higher order SMO or adaptive SMO are adopted in the position sensorless control, it usually involved multiple designed parameters. Since the performance of SMO is sensitive to the setting of these parameters, extra work is required to tune the observer to achieve the desired performance. But at the same time, the main advantage of SMO, namely its simple algorithm, should not be compromised.

The linear sliding surface in the SMO only guarantees the asymptotic stability of the system in the sliding mode. This would mean that the system states converge to the origin, but at an infinite time. Therefore, nonlinear sliding surfaces, such as terminal sliding surface, have been introduced in the SMO design in recent years. However, the stability proof of these observers is conducted in a continuous-time domain. As discussed in [116], the finite-time convergence behavior observed in continuous-time TSM is lost with discretization. It is also shown that discretization would lead to a periodic behavior and even instability in certain cases. Therefore, during the discrete-time design of SMO, the stability condition should be carefully addressed, especially when nonlinear sliding surface is involved.

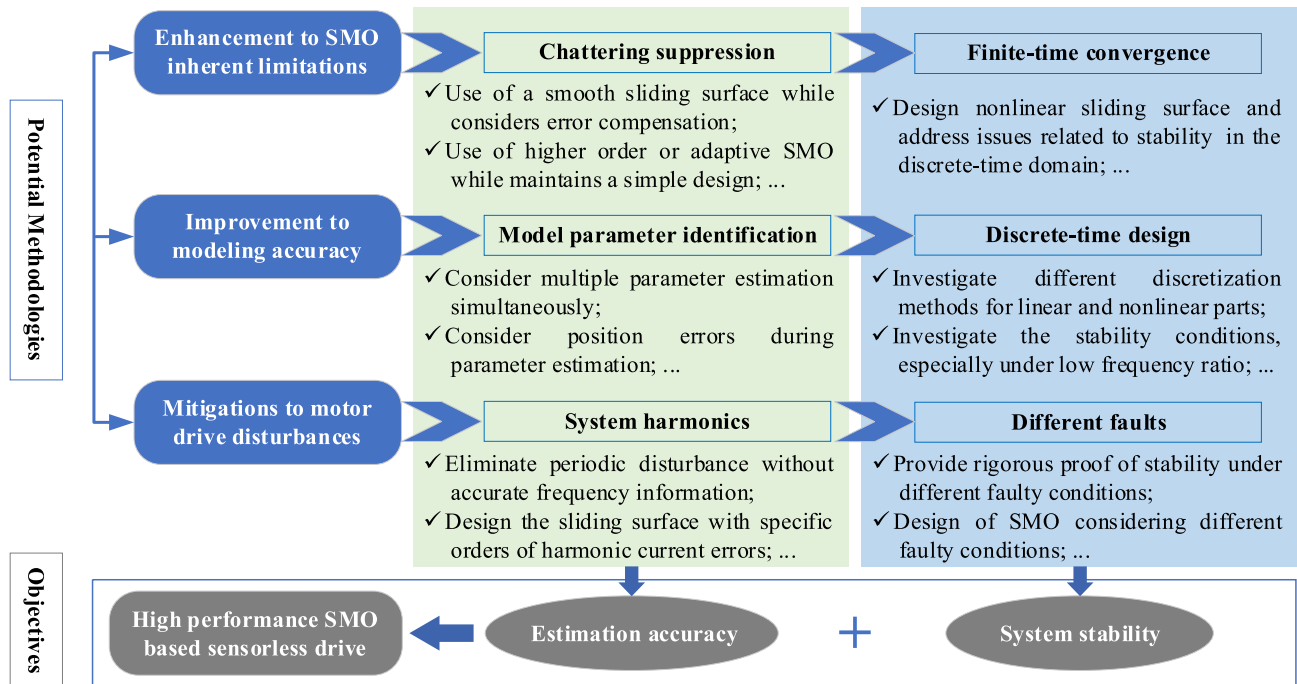


Fig. 12. Future outlook for SMO-based PMSM position sensorless control.

### B. Improvement to Modeling Accuracy

Under heavy load conditions, where stator currents are high,  $dq$ -axis inductance variations due to magnetic saturation will bring chattering and offset in the estimated position. Additionally, the resistance mismatch can also lead to a position error in the low-speed region. However, existing parameter correction methods mainly consider  $q$ -axis inductance and resistance identification, while  $d$ -axis inductance mismatch is usually ignored. Therefore, in order to achieve high-performance SMO-based sensorless control, it is necessary to consider multiparameter identification. Moreover, most of the existing methods consider the position estimation error as zero during parameter identification, which is not true. Therefore, the future work needs to consider the existing position error during the parameter identification.

Existing work has shown that DSMO design with traditional Euler approximation will almost lose stability when frequency ratio is lower than 8 [93]. To extend SMO stability range at low-frequency ratio conditions, advanced discretization methods have been used in the SMO design. For example, existing work has shown that the SMO can operate at a frequency ratio of 5 with advanced filtering techniques and direct discrete-time domain design [89]. However, the complex calculation in the DSMO cannot be ignored. Although the trigonometric and exponential operations can be performed through lookup tables, it still takes up storage space. One possible solution is to decouple the PMSM model during the discrete-time design of SMO. For example, the PMSM can be divided with Hammerstein model or Wiener model into two parts: static nonlinearity part and linear dynamics part. Based on the characteristics of each part, different discretization methods can be used, instead of directly using

complicated exact discretization for the whole machine model. Furthermore, most of the existing work directly uses different discretization methods for DSMO design. However, it should be noted that the DSMO design cannot be directly converted from its continuous counterpart through simple equivalence. DSMO can undergo only quasi-sliding mode motion, i.e., the system states may approach the sliding surface but are generally incapable of staying on it. Therefore, during the discrete-time design of SMO, the stability condition should be carefully addressed.

### C. Mitigations to Motor Drive Disturbances

Different harmonics exist in the motor drive system and they can reduce SMO performance to a large extent. For example, inverter nonlinearity causes sixth-order harmonics in the drive system, and it is also the main factor limiting the performance of the SMO in the low-speed region. Although many methods have been proposed in recent years to compensate for these harmonics, they rarely consider the compensation performance in the presence of position errors. For filter-based methods, they usually require speed information to filter out the specific harmonic. The performance may be degraded, when the estimated speed cannot perfectly track the real speed. Therefore, it is necessary to deal with periodic disturbances without accurate frequency information. In addition, how to deal with the chattering aggravated by distorted current signals is still an open topic. It may be possible to design the sliding surface which considers the specific order of harmonic current errors.

Although SMO has a good robustness to measurement errors compared to linear observers, its performance under different levels of current measurement fault still needs to be analyzed and quantified. There is potential loss of observability when some of



the current measurements are not available. Some SMO-based single current sensor strategies have been proposed in recent years for position sensorless control of PMSM drives [117], [118]. In these methods, the current reconstruction needs the involvement of the estimated speed or rotor position information. Thereafter, the reconstructed current is used for speed and position estimation, which would lead to undesired coupling effects. Hence, rigorous proof of stability on this topic is essential. In addition, the design of SMO under machine faulty conditions is still an open topic. For example, when an interturn short-circuit fault exists, the structure of SMO needs to be redesigned considering the possible changes in the dimension of the machine model to avoid the potential loss of stability. This opens the opportunity for future researchers to explore the combination of SMO with other fault tolerant control techniques.

## VI. CONCLUSION

An extensive review of the state-of-the-art implementation of SMO for position sensorless control of PMSMs is presented in this article. Various sliding surface and control law designs have been investigated and compared. The remarkable advantages as well as the disadvantages of previous article are summarized. Additionally, the design of SMO under nonideal conditions is reviewed. Ideas on possible future work are also discussed, which emphasize current gaps in this area of research. This article aims to introduce the technical knowledge of SMO-based sensorless control from both theoretical and practical implementation perspectives for its widespread use in the electric motor drive area.

## APPENDIX A

### ACTIVE FLUX MODEL FOR PMSMS

The “AF” concept proposed by Boldea et al. [7] turns all rotor salient-pole ac machines into fictitious rotor nonsalient-pole machines such that the rotor position and speed estimations become simpler. For the PMSM, the AF linkage is defined as

$$\begin{cases} T_e = 1.5N_p\psi_{af}i_q \\ \psi_{af} = (L_d - L_q)i_d + \psi_f \end{cases} \quad (39)$$

where  $T_e$  is electromagnetic torque;  $N_p$  is the pole pair;  $\psi_{af}$  in (39) is defined as “AF” or “extended rotor flux” [8] or “equivalent EMF” [9], which comprises two parts: the conventional permanent-magnet flux linkage  $\psi_f$  and the flux linkage due to the saliency. Based on the definition,  $\psi_{af}$  always lies on the  $d$ -axis, which guarantees the AF model can be successfully applied in any operation mode.

As per Faraday’s law with the transformation of  $\psi_{af}$  into  $\alpha\beta$ -axis, the AF model of the PMSM can be derived as

$$\begin{aligned} \mathbf{u}_{\alpha\beta} = & \begin{bmatrix} R_s & 0 \\ 0 & R_s \end{bmatrix} \mathbf{i}_{\alpha\beta} + \frac{d\mathbf{i}_{\alpha\beta}}{dt} \begin{bmatrix} L_q & 0 \\ 0 & L_q \end{bmatrix} \\ & + \frac{d}{dt} \left( \psi_{af} \begin{bmatrix} \cos(\theta_e) \\ \sin(\theta_e) \end{bmatrix} \right). \end{aligned} \quad (40)$$

The comparison of EEMF model and AF model in the stationary frame is summarized in Table III. For a nonsalient

TABLE III  
COMPARISON OF EEMF MODEL AND AF MODEL FOR PMSMS IN THE STATIONARY FRAME [119]

Model terms	EEMF model	AF model
Impedance matrix	$\begin{bmatrix} R_s & -\omega_e L_\Delta \\ \omega_e L_\Delta & R_s \end{bmatrix}$	$\begin{bmatrix} R_s & 0 \\ 0 & R_s \end{bmatrix}$
Inductance matrix	$\begin{bmatrix} L_d & 0 \\ 0 & L_d \end{bmatrix}$	$\begin{bmatrix} L_q & 0 \\ 0 & L_q \end{bmatrix}$
Position related terms	$E_{ex} \begin{bmatrix} -\sin\theta_e \\ \cos\theta_e \end{bmatrix}$	$\frac{d}{dt}(\psi_{af} \begin{bmatrix} \cos(\theta_e) \\ \sin(\theta_e) \end{bmatrix})$

PMSM with  $L_d = L_q$ , the AF model is equal to EEMF model considering a constant flux. For an interior PMSM, the AF model has no cross coupling, no dependency on the  $d$ -axis inductance and permanent magnet flux linkage, when compared with the EEMF model. Hence, the AF model has better robustness against parameter variation and external load change. However, an integrator is directly required to calculate the AF components, from which the rotor position can be extracted. Therefore, some practical issues, e.g., integrator dc offset and initial condition, should be carefully handled for an interior PMSM.

The AF model can also be derived in the rotating reference frame as

$$\begin{aligned} \mathbf{u}_{dq} = & \begin{bmatrix} R_s & -\omega_e L_q \\ \omega_e L_q & R_s \end{bmatrix} \mathbf{i}_{dq} + \frac{d\mathbf{i}_{dq}}{dt} \begin{bmatrix} L_q & 0 \\ 0 & L_q \end{bmatrix} \\ & + \begin{bmatrix} \frac{d\psi_{af}}{dt} \\ \omega_e \psi_{af} \end{bmatrix}. \end{aligned} \quad (41)$$

Compared (40) with (41), the AF model in the stationary frame does not require speed information in the model, so AF model in the stationary frame is dominantly used in the position sensorless control of PMSMs.

## REFERENCES

- [1] H. Kim, J. Son, and J. Lee, “A high-speed sliding-mode observer for the sensorless speed control of a PMSM,” *IEEE Trans. Ind. Electron.*, vol. 58, no. 9, pp. 4069–4077, Sep. 2011.
- [2] W. Xu, S. Qu, L. Zhao, and H. Zhang, “An improved adaptive sliding mode observer for middle- and high-speed rotor tracking,” *IEEE Trans. Power Electron.*, vol. 36, no. 1, pp. 1043–1053, Jan. 2021.
- [3] A. K. Junejo, W. Xu, C. Mu, M. M. Ismail, and Y. Liu, “Adaptive speed control of PMSM drive system based a new sliding-mode reaching law,” *IEEE Trans. Power Electron.*, vol. 35, no. 11, pp. 12110–12121, Nov. 2020.
- [4] M. Pacas, “Sensorless drives in industrial applications,” *IEEE Ind. Electron. Mag.*, vol. 5, no. 2, pp. 16–23, Jun. 2011.
- [5] N. Bianchi and S. Bolognani, “Influence of rotor geometry of an IPM motor on sensorless control feasibility,” *IEEE Trans. Ind. Appl.*, vol. 43, no. 1, pp. 87–96, Jan./Feb. 2007.
- [6] Z. Chen, M. Tomita, S. Doki, and S. Okuma, “An extended electromotive force model for sensorless control of interior permanent-magnet synchronous motors,” *IEEE Trans. Ind. Electron.*, vol. 50, no. 2, pp. 288–295, Apr. 2003.
- [7] I. Boldea, M. C. Paicu, and G. D. Andreescu, “Active flux concept for motion-sensorless unified AC drives,” *IEEE Trans. Power Electron.*, vol. 23, no. 5, pp. 2612–2618, Sep. 2008.
- [8] G. Foo and M. F. Rahman, “Sensorless direct torque and flux-controlled IPM synchronous motor drive at very low speed without signal injection,” *IEEE Trans. Ind. Electron.*, vol. 57, no. 1, pp. 395–403, Jan. 2010.

- [9] J. Liu, T. A. Nondahl, P. B. Schmidt, S. Royak, and M. Harbaugh, "Rotor position estimation for synchronous machines based on equivalent EMF," *IEEE Trans. Ind. Appl.*, vol. 47, no. 3, pp. 1310–1318, May/Jun. 2011.
- [10] Y. Zhao, Z. Zhang, W. Qiao, and L. Wu, "An Extended flux model-based rotor position estimator for sensorless control of salient-pole permanent-magnet synchronous machines," *IEEE Trans. Power Electron.*, vol. 30, no. 8, pp. 4412–4422, Aug. 2015.
- [11] K.-B. Lee and F. Blaabjerg, "Reduced-order extended Luenberger observer based sensorless vector control driven by matrix converter with nonlinearity compensation," *IEEE Trans. Ind. Electron.*, vol. 53, no. 1, pp. 66–75, Feb. 2006.
- [12] A. Andersson and T. Thiringer, "Motion sensorless IPMSM control using linear moving horizon estimation with Luenberger observer state feedback," *IEEE Trans. Transp. Electrification*, vol. 4, no. 2, pp. 464–473, Jun. 2018.
- [13] P. Kshirsagar et al., "Implementation and sensorless vector-control design and tuning strategy for SMPM machines in fan-type applications," *IEEE Trans. Ind. Appl.*, vol. 48, no. 6, pp. 2402–2413, Nov./Dec. 2012.
- [14] C. Wu, Z. Chen, and Q. Chen, "Hybrid-modulation-based full-speed sensorless control for permanent magnet synchronous motors," *IEEE Trans. Power Electron.*, vol. 37, no. 5, pp. 5908–5917, May 2022.
- [15] F. Parasiliti, R. Petrella, and M. Tursini, "Sensorless speed control of a PM synchronous motor by sliding mode observer," in *Proc. IEEE Int. Symp. Ind. Electron.*, 1997, pp. 1106–1111.
- [16] N. K. Quang, N. T. Hieu, and Q. P. Ha, "FPGA-based sensorless PMSM speed control using reduced-order extended Kalman filters," *IEEE Trans. Ind. Electron.*, vol. 61, no. 12, pp. 6574–6582, Dec. 2014.
- [17] Z. Wang, Y. Zheng, Z. Zou, and M. Cheng, "Position sensorless control of interleaved CSI fed PMSM drive with extended Kalman filter," *IEEE Trans. Magn.*, vol. 48, no. 11, pp. 3688–3691, Nov. 2012.
- [18] Y.-H. Kim and Y.-S. Kook, "High performance IPMSM drives without rotational position sensors using reduced-order EKF," *IEEE Trans. Energy Convers.*, vol. 14, no. 4, pp. 868–873, Dec. 1999.
- [19] Z. Yin, F. Gao, Y. Zhang, C. Du, G. Li, and X. Sun, "A review of nonlinear Kalman filter applying to sensorless control for AC motor drives," *CES Trans. Elect. Mach. Syst.*, vol. 3, no. 4, pp. 351–362, Dec. 2019.
- [20] V. I. Utkin, "Sliding mode control design principles and applications to electric drives," *IEEE Trans. Ind. Electron.*, vol. 40, no. 1, pp. 23–36, Feb. 1993.
- [21] G. Tang, Z. Xu, H. Dong, and Q. Xu, "Sliding mode robust control based active-power modulation of multi-terminal HVDC transmissions," *IEEE Trans. Power Syst.*, vol. 31, no. 2, pp. 1614–1623, Mar. 2016.
- [22] L. Zhang, Z. Chen, X. Yu, J. Yang, and S. Li, "Sliding-mode-based robust output regulation and its application in PMSM servo systems," *IEEE Trans. Ind. Electron.*, vol. 70, no. 2, pp. 1852–1860, Feb. 2023.
- [23] S. Lin and W. Zhang, "An adaptive sliding-mode observer with a tangent function-based PLL structure for position sensorless PMSM drives," *Int. J. Elect. Power Energy Syst.*, vol. 88, pp. 63–74, 2017.
- [24] Y. Zhong, H. Lin, J. Wang, and H. Yang, "Improved adaptive sliding mode observer based position sensorless control for variable flux memory machines," *IEEE Trans. Power Electron.*, vol. 38, no. 5, pp. 6395–6406, May 2023.
- [25] Y. Zhang and J. Liu, "An improved Q-PLL to overcome the speed reversal problems in sensorless PMSM drive," in *Proc. IEEE 8th Int. Power Electron. Motion Control Conf.*, 2016, pp. 1884–1888.
- [26] S. Morimoto, K. Kawamoto, M. Sanada, and Y. Takeda, "Sensorless control strategy for salient-pole PMSM based on extended EMF in rotating reference frame," *IEEE Trans. Ind. Appl.*, vol. 38, no. 4, pp. 1054–1061, Jul./Aug. 2002.
- [27] M. Furat and I. Eker, "Experimental evaluation of sliding mode control techniques," *J. Fac. Eng. Architecture*, vol. 27, no. 1, pp. 23–37, 2012.
- [28] C. Volosencu, K. Serdar, G. Jose, and O. Valero, *Automation and Control*. London, U.K.: IntechOpen, 2021.
- [29] J. Farrell and M. M. Polycarpou, *Adaptive Approximation Based Control: Unifying Neural, Fuzzy and Traditional Adaptive Approximation Approaches*. Hoboken, NJ, USA: Wiley Interscience, 2006.
- [30] S. Chi, Z. Zhang, and L. Xu, "Sliding-mode sensorless control of direct-drive PM synchronous motors for washing machine applications," *IEEE Trans. Ind. Appl.*, vol. 45, no. 2, pp. 582–590, Mar./Apr. 2009.
- [31] X. Zhang, "Sensorless induction motor drive using indirect vector controller and sliding-mode observer for electric vehicles," *IEEE Trans. Veh. Technol.*, vol. 62, no. 7, pp. 3010–3018, Sep. 2013.
- [32] K.-L. Kang, J.-M. Kim, K.-B. Hwang, and K.-H. Kim, "Sensorless control of PMSM in high speed range with iterative sliding mode observer," in *Proc. 19th Annu. Appl. Power Electron. Conf.*, 2004, pp. 1111–1116.
- [33] L. Sheng, W. Li, Y. Wang, M. Fan, and X. Yang, "Sensorless control of a shearer short-range cutting interior permanent magnet synchronous motor based on a new sliding mode observer," *IEEE Access*, vol. 5, pp. 18439–18450, 2017.
- [34] V. Srikanth and A. A. Dutt, "A comparative study on the effect of switching functions in SMO for PMSM drives," in *Proc. IEEE Int. Conf. Power Electron., Drives Energy Syst.*, 2012, pp. 1–6.
- [35] J. J. E. Slotine and S. S. Sastry, "Tracking control of nonlinear systems using sliding surfaces, with application to robot manipulators," in *Proc. Amer. Control Conf.*, 1983, pp. 132–135.
- [36] S. Ye and X. Yao, "An enhanced SMO-based permanent-magnet synchronous machine (PMSM) sensorless drive scheme with current measurement error compensation," *IEEE J. Emerg. Sel. Topics Power Electron.*, vol. 9, no. 4, pp. 4407–4419, Aug. 2021.
- [37] Z. Yin, Y. Zhang, X. Cao, D. Yuan, and J. Liu, "Estimated position error suppression using novel PLL for IPMSM sensorless drives based on full-order SMO," *IEEE Trans. Power Electron.*, vol. 37, no. 4, pp. 4463–4474, Apr. 2022.
- [38] G. Wang, Z. Li, G. Zhang, Y. Yu, and D. Xu, "Quadrature PLL-based high order sliding-mode observer for IPMSM sensorless control with online MTPA control strategy," *IEEE Trans. Energy Convers.*, vol. 28, no. 1, pp. 214–224, Mar. 2013.
- [39] W. Xu, S. Qu, J. Zhao, H. Zhang, and X. Du, "An improved full-order sliding-mode observer for rotor position and speed estimation of SPMSM," *IEEE Access*, vol. 9, pp. 15099–15109, 2021.
- [40] V. C. Ilioudis, "Chattering reduction applied in PMSM sensorless control using second order sliding mode observer," in *Proc. 9th Int. Conf. Compat. Power Electron.*, 2015, pp. 240–245.
- [41] S. Di Gennaro, J. Rivera Domínguez, and M. A. Meza, "Sensorless high order sliding mode control of induction motors with core loss," *IEEE Trans. Ind. Electron.*, vol. 61, no. 6, pp. 2678–2689, Jun. 2014.
- [42] H. Wang, X. Ge, and Y. Liu, "Second-order sliding-mode MRAS observer-based sensorless vector control of linear induction motor drives for medium-low speed maglev applications," *IEEE Trans. Ind. Electron.*, vol. 65, no. 12, pp. 9938–9952, Dec. 2018.
- [43] Z. Li, S. Zhou, Y. Xiao, and L. Wang, "Sensorless vector control of permanent magnet synchronous linear motor based on self-adaptive super-twisting sliding mode controller," *IEEE Access*, vol. 7, pp. 44998–45011, 2019.
- [44] L. Zhao, J. Huang, H. Liu, B. Li, and W. Kong, "Second-order sliding-mode observer with online parameter identification for sensorless induction motor drives," *IEEE Trans. Ind. Electron.*, vol. 61, no. 10, pp. 5280–5289, Oct. 2014.
- [45] X. Lin et al., "Observer-based fixed-time control for permanent-magnet synchronous motors with parameter uncertainties," *IEEE Trans. Power Electron.*, vol. 38, no. 4, pp. 4335–4344, Apr. 2023.
- [46] T. Wang, B. Wang, Y. Yu, and D. Xu, "Discrete sliding-mode-based MRAS for speed-sensorless induction motor drives in the high-speed range," *IEEE Trans. Power Electron.*, vol. 38, no. 5, pp. 5777–5790, May 2023.
- [47] A. Levant, "Robust Exact differentiation via sliding mode technique," *Automatica*, vol. 34, no. 3, pp. 379–384, Mar. 1998.
- [48] V. Utkin, "On convergence time and disturbance rejection of super-twisting control," *IEEE Trans. Autom. Control*, vol. 58, no. 8, pp. 2013–2017, Aug. 2013.
- [49] B. Wang, T. Wang, Y. Yu, C. Luo, and D. Xu, "Convergence trajectory optimization of super-twisting sliding-mode current control for induction motor drives," *IEEE Trans. Ind. Electron.*, vol. 69, no. 12, pp. 12292–12304, Dec. 2022.
- [50] W. A. Teklu and X. Ge, "Speed sensorless control of IPMSM using super-twisted sliding mode observer based integral backstepping theory," in *Proc. IEEE Int. Power Electron. Appl. Conf. Expo.*, 2018, pp. 1–6.
- [51] D. Liang, J. Li, R. Qu, and W. Kong, "Adaptive second-order sliding-mode observer for PMSM sensorless control considering VSI nonlinearity," *IEEE Trans. Power Electron.*, vol. 33, no. 10, pp. 8994–9004, Oct. 2018.
- [52] Y. Zhao, W. Qiao, and L. Wu, "An adaptive quasi-sliding-mode rotor position observer-based sensorless control for interior permanent magnet synchronous machines," *IEEE Trans. Power Electron.*, vol. 28, no. 12, pp. 5618–5629, Dec. 2013.
- [53] Z. Chen, A. A. Dawara, X. Zhang, H. Zhang, C. Liu, and G. Luo, "Adaptive sliding mode observer-based sensorless control for SPMSM employing a dual-PLL," *IEEE Trans. Transp. Electrification*, vol. 8, no. 1, pp. 1267–1277, Mar. 2021.

- [54] M. Gaballah, M. E. Bardini, and M. Sharaf, "Chattering-free sliding mode observer for speed sensorless control of PMSM," *Appl. Comput. Inform.*, vol. 13, pp. 169–174, 2017.
- [55] S. Ye, "Fuzzy sliding mode observer with dual SOGI-FLL in sensorless control of PMSM drives," *ISA Trans.*, vol. 85, pp. 161–176, Feb. 2019.
- [56] C. Wang and D. Cao, "New sensorless speed control of a hybrid stepper motor based on fuzzy sliding mode observer," *Energies*, vol. 13, no. 18, Sep. 2020, Art. no. 4939.
- [57] J. Lee, P. H. Chang, and M. Jin, "Adaptive integral sliding mode control with time-delay estimation for robot manipulators," *IEEE Trans. Ind. Electron.*, vol. 64, no. 8, pp. 6796–6804, Aug. 2017.
- [58] A. Bessas, A. Benalia, and F. Boudjema, "Integral sliding mode control for trajectory tracking of wheeled mobile robot in presence of uncertainties," *J. Control Sci. Eng.*, vol. 2016, May 2016, Art. no. 250140.
- [59] J. Yang, S. Li, and X. Yu, "Sliding-mode control for systems with mismatched uncertainties via a disturbance observer," *IEEE Trans. Ind. Electron.*, vol. 60, no. 1, pp. 160–169, Jan. 2013.
- [60] F. Wang and L. He, "FPGA-based predictive speed control for pmsm system using integral sliding-mode disturbance observer," *IEEE Trans. Ind. Electron.*, vol. 68, no. 2, pp. 972–981, Feb. 2021.
- [61] S. T. Venkataraman and S. Gulati, "Control of nonlinear systems using terminal sliding modes," in *Proc. Amer. Control Conf.*, 1992, pp. 891–893.
- [62] S. Li, M. Zhou, and X. Yu, "Design and implementation of terminal sliding mode control method for PMSM speed regulation system," *IEEE Trans. Ind. Inform.*, vol. 9, no. 4, pp. 1879–1891, Nov. 2013.
- [63] Y. Feng, J. Zheng, X. Yu, and N. V. Truong, "Hybrid terminal sliding-mode observer design method for a permanent-magnet synchronous motor control system," *IEEE Trans. Ind. Electron.*, vol. 56, no. 9, pp. 3424–3431, Sep. 2009.
- [64] Y. Feng, X. Yu, and F. Han, "On nonsingular terminal sliding-mode control of nonlinear systems," *Automatica*, vol. 49, no. 6, pp. 1715–1722, 2013.
- [65] L. Yang and J. Yang, "Nonsingular fast terminal sliding-mode control for nonlinear dynamical systems," *Int. J. Robust Nonlinear Control*, vol. 21, no. 16, pp. 1865–1879, 2011.
- [66] B. Xu, L. Zhang, and W. Ji, "Improved non-singular fast terminal sliding mode control with disturbance observer for PMSM drives," *IEEE Trans. Transp. Electric.*, vol. 7, no. 4, pp. 2753–2762, Dec. 2021.
- [67] T.-N. Nguyen, T.-B. Pham, V.-T. Hoang, T.-T. Nguyen, V.-L. Nguyen, and N.-V. Truong, "Efficient sensorless speed estimation of electrical servo drives using a full-order nonsingular terminal sliding mode observer," *Math. Problems Eng.*, vol. 2021, pp. 1–8, 2021.
- [68] S. Yu, X. Yu, B. Shirinzadeh, and Z. Man, "Continuous finite-time control for robotic manipulators with terminal sliding mode," *Automatica*, vol. 41, no. 11, pp. 1957–1964, Nov. 2005.
- [69] B. Wang, Y. Shao, Y. Yu, Q. Dong, Z. Yun, and D. G. Xu, "High-order terminal sliding-mode observer for chattering suppression and finite-time convergence in sensorless SPMSM drives," *IEEE Trans. Power Electron.*, vol. 36, no. 10, pp. 11910–11920, Oct. 2021.
- [70] D. Krupp and Y.-B. Shtessel, "Chattering-free sliding mode control with unmodeled dynamics," in *Proc. Amer. Control Conf.*, 1999, pp. 530–534.
- [71] S. Bolognani, L. Ortolina, F. Tinazzi, and M. Zigliotto, "Model sensitivity of fundamental-frequency-based position estimators for sensorless PM and reluctance synchronous motor drives," *IEEE Trans. Ind. Electron.*, vol. 65, no. 1, pp. 77–85, Jan. 2018.
- [72] D. Xiao et al., "Universal full-speed sensorless control scheme for interior permanent magnet synchronous motors," *IEEE Trans. Power Electron.*, vol. 36, no. 4, pp. 4723–4737, Apr. 2021.
- [73] G. Zhang, H. Zhou, G. Wang, C. Li, and D. Xu, "Current Sensor fault-tolerant control for encoderless IPMSM drives based on current space vector error reconstruction," *IEEE J. Emerg. Sel. Topics Power Electron.*, vol. 8, no. 4, pp. 3658–3668, Dec. 2020.
- [74] L. Zhao, J. Huang, H. Liu, B. Li, and W. Kong, "Second-order sliding-mode observer with online parameter identification for sensorless induction motor drives," *IEEE Trans. Ind. Electron.*, vol. 61, no. 10, pp. 5280–5289, Oct. 2014.
- [75] Y. Inoue, Y. Kawaguchi, S. Morimoto, and M. Sanada, "Performance improvement of sensorless IPMSM drives in a low-speed region using online parameter identification," *IEEE Trans. Ind. Appl.*, vol. 47, no. 2, pp. 798–804, Mar. 2011.
- [76] P. Phowanna, S. Boonto, E. Mujjalinvimut, M. Konghirun, and W. Lenwari, "Improved performance of sliding mode observer using parameter adaptation in sensorless IPMSM drive," in *Proc. 12th IEEE Conf. Ind. Electron. Appl.*, 2017, pp. 1635–1640.
- [77] M. Hasegawa and K. Matsui, "Position sensorless control for interior permanent magnet synchronous motor using adaptive flux observer with inductance identification," *IET Elect. Power Appl.*, vol. 3, no. 3, pp. 209–217, May 2009.
- [78] K. Liu, Q. Zhang, J. T. Chen, Z. Q. Zhu, J. Zhang, and A. W. Shen, "Online multiparameter estimation of non-salient pole PM synchronous machines with temperature variation tracking," *IEEE Trans. Ind. Electron.*, vol. 58, no. 5, pp. 1776–1788, May 2011.
- [79] C. Wu, Y. Zhao, and M. Sun, "Enhancing low-speed sensorless control of PMSM using phase voltage measurements and online multiple parameter identification," *IEEE Trans. Power Electron.*, vol. 35, no. 10, pp. 10700–10710, Oct. 2020.
- [80] M. Hasegawa and K. Matsui, "Position sensorless control for interior permanent magnet synchronous motor using adaptive flux observer with inductance identification," *IET Elect. Power Appl.*, vol. 3, no. 3, pp. 209–217, Apr. 2009.
- [81] M. S. Rafiq, J. K. F. Mwasilu, H. H. Choi, and J. Jung, "Online parameter identification for model-based sensorless control of interior permanent magnet synchronous machine," *IEEE Trans. Power Electron.*, vol. 32, no. 6, pp. 4631–4643, Jun. 2017.
- [82] D. Q. Dang, M. S. Rafiq, H. H. Choi, and J. W. Jung, "Online parameter estimation technique for adaptive control applications of interior PM synchronous motor drives," *IEEE Trans. Ind. Electron.*, vol. 63, no. 3, pp. 1438–1449, Mar. 2016.
- [83] F. Zhou and D. G. Fisher, "Continuous sliding mode control," *Int. J. Control*, vol. 55, pp. 313–327, 1992.
- [84] A. Bartoszewicz, "Discrete-time quasi-sliding-mode control strategies," *IEEE Trans. Ind. Electron.*, vol. 42, no. 2, pp. 117–122, Apr. 1995.
- [85] S. Janardhanan and B. Bandyopadhyay, "Multirate output feedback based robust quasi-sliding mode control of discrete-time systems," *IEEE Trans. Automat. Control*, vol. 52, no. 3, pp. 499–503, Mar. 2007.
- [86] Q. An, J. Zhang, Q. An, and A. Shamekov, "Quasi-proportional-resonant controller based adaptive position observer for sensorless control of PMSM drives under low frequency ratio," *IEEE Trans. Ind. Electron.*, vol. 67, no. 4, pp. 2564–2573, Apr. 2020.
- [87] Y. Zhao, W. Qiao, and L. Wu, "Sensorless control for IPMSMs based on a multilayer discrete-time sliding-mode observer," in *Proc. IEEE Energy Convers. Congr. Expo.*, 2012, pp. 1788–1795.
- [88] T. Bernardes, V. F. Montagner, H. A. Gründling, and H. Pinheiro, "Discrete-time sliding mode observer for sensorless vector control of permanent magnet synchronous machine," *IEEE Trans. Ind. Electron.*, vol. 61, no. 4, pp. 1679–1691, Apr. 2014.
- [89] Y. Zhang, Z. Yin, X. Cao, Y. Zhang, and J. Liu, "A novel SPMSM sensorless drive using discrete-time synchronous-frequency adaptive observer under low frequency ratio," *IEEE Trans. Power Electron.*, vol. 37, no. 9, pp. 11045–11057, Sep. 2022.
- [90] L. V. Gera, G. Botto, L. D. Suarez Cabrera, and M. Chiaberge, "Advanced sensorless control system for PMSM-based automotive application," in *Proc. 16th Eur. Conf. Power Electron. Appl.*, 2014, pp. 1–8.
- [91] B. Wang, Y. Zhao, Y. Yu, G. Wang, D. Xu, and Z. Dong, "Speed-sensorless induction machine control in the field-weakening region using discrete speed-adaptive full-order observer," *IEEE Trans. Power Electron.*, vol. 31, no. 8, pp. 5759–5773, Aug. 2016.
- [92] L. Ding, Y. W. Li, and N. R. Zargari, "Discrete-time SMO sensorless control of current source converter-fed PMSM drives with low switching frequency," *IEEE Trans. Ind. Electron.*, vol. 68, no. 3, pp. 2120–2129, Mar. 2021.
- [93] G. Zhang, G. Wang, D. Xu, and Y. Yu, "Discrete-time low-frequency-ratio synchronous-frame full-order observer for position sensorless IPMSM drives," *IEEE J. Emerg. Sel. Topics Power Electron.*, vol. 5, no. 2, pp. 870–879, Jun. 2017.
- [94] L. Ding, Y. W. Li, N. R. Zargari, and R. Paes, "Sensorless control of CSC-fed PMSM drives with low switching frequency for electrical submersible pump application," *IEEE Trans. Ind. Appl.*, vol. 56, no. 4, pp. 3799–3808, Jul./Aug. 2020.
- [95] S.-Y. Kim and S.-Y. Park, "Compensation of dead-time effects based on adaptive harmonic filtering in the vector-controlled AC motor drives," *IEEE Trans. Ind. Electron.*, vol. 54, no. 3, pp. 1768–1777, Jun. 2007.
- [96] G. Feng, C. Lai, K. Mukherjee, and N. C. Kar, "Current injection-based online parameter and VSI nonlinearity estimation for PMSM drives using current and voltage DC components," *IEEE Trans. Transp. Electric.*, vol. 2, no. 2, pp. 119–128, Jun. 2016.
- [97] X. Ding et al., "Analytical and experimental evaluation of SiC-inverter nonlinearities for traction drives used in electric vehicles," *IEEE Trans. Veh. Technol.*, vol. 67, no. 1, pp. 146–159, Jan. 2018.



- [98] G. Zhang, G. Wang, D. Xu, and N. Zhao, "ADALINE-network-based PLL for position sensorless interior permanent magnet synchronous motor drives," *IEEE Trans. Power Electron.*, vol. 31, no. 2, pp. 1450–1460, Feb. 2016.
- [99] X. Wu et al., "Complex-coefficient synchronous frequency filter-based position estimation error reduction for sensorless IPMSM drives," *IEEE Trans. Power Electron.*, vol. 37, no. 12, pp. 15297–15307, Dec. 2022.
- [100] T. Wu, X. Wu, S. Huang, K. Lu, and H. Cui, "An optimized PLL with time delay and harmonic suppression for improved position estimation accuracy of PMSM based on Levenberg–Marquardt," *IEEE Trans. Ind. Electron.*, vol. 70, no. 10, pp. 9847–9858, Oct. 2023.
- [101] N. Urasaki, T. Senjyu, K. Uezato, and T. Funabashi, "Adaptive dead-time compensation strategy for permanent magnet synchronous motor drive," *IEEE Trans. Energy Convers.*, vol. 22, no. 2, pp. 271–280, Jun. 2007.
- [102] K. J. Lee, B. G. Park, R. Y. Kim, and D. S. Hyun, "Robust predictive current controller based on a disturbance estimator in a three-phase grid-connected inverter," *IEEE Trans. Power Electron.*, vol. 27, no. 1, pp. 276–283, Jan. 2012.
- [103] M. A. Herran, J. R. Fischer, S. A. Gonzalez, M. G. Judewicz, and D. O. Carrica, "Adaptive dead-time compensation for grid-connected PWM inverters of single-stage PV systems," *IEEE Trans. Power Electron.*, vol. 28, no. 6, pp. 2816–2825, Jun. 2013.
- [104] Y. Wang, Y. Xu, and J. Zou, "Sliding-mode sensorless control of PMSM with inverter nonlinearity compensation," *IEEE Trans. Power Electron.*, vol. 34, no. 10, pp. 10206–10220, Oct. 2019.
- [105] X. Song, J. Fang, B. Han, and S. Zheng, "Adaptive compensation method for high-speed surface PMSM sensorless drives of EMF-based position estimation error," *IEEE Trans. Power Electron.*, vol. 31, no. 2, pp. 1438–1449, Feb. 2016.
- [106] Y. Wang, Y. Xu, and J. Zou, "ILC-based voltage compensation method for PMSM sensorless control considering inverter nonlinearity and sampling current DC bias," *IEEE Trans. Ind. Electron.*, vol. 67, no. 7, pp. 5980–5989, Jul. 2020.
- [107] D. Liang, J. Li, R. Qu, and W. Kong, "Adaptive second-order sliding-mode observer for PMSM sensorless control considering VSI nonlinearity," *IEEE Trans. Power Electron.*, vol. 33, no. 10, pp. 8994–9004, Oct. 2018.
- [108] H. Zhao, Q. M. J. Wu, and A. Kawamura, "An accurate approach of nonlinearity compensation for VSI inverter output voltage," *IEEE Trans. Power Electron.*, vol. 19, no. 4, pp. 1029–1035, Jul. 2004.
- [109] S. Hwang and J. Kim, "Dead time compensation method for voltage-fed PWM inverter," *IEEE Trans. Energy Convers.*, vol. 25, no. 1, pp. 1–10, Mar. 2010.
- [110] D. Park and K. Kim, "Parameter-independent online compensation scheme for dead time and inverter nonlinearity in IPMSM drive through waveform analysis," *IEEE Trans. Ind. Electron.*, vol. 61, no. 2, pp. 701–707, Feb. 2014.
- [111] P. Vaclavek, P. Blaha, and I. Herman, "AC drive observability analysis," *IEEE Trans. Ind. Electron.*, vol. 60, no. 8, pp. 3047–3059, Aug. 2013.
- [112] S.-K. Sul, Y.-C. Kwon, and Y. Lee, "Sensorless control of IPMSM for last 10 years and next 5 years," *CES Trans. Elect. Mach. Syst.*, vol. 1, no. 2, pp. 91–99, 2017.
- [113] J. Lara, J. Xu, and A. Chandra, "Effects of rotor position error in the performance of field-oriented-controlled PMSM drives for electric vehicle traction applications," *IEEE Trans. Ind. Electron.*, vol. 63, no. 8, pp. 4738–4751, Aug. 2016.
- [114] B. Shuang, Z. Q. Zhu, and X. Wu, "Improved cross-coupling effect compensation method for sensorless control of IPMSM with high frequency voltage injection," *IEEE Trans. Energy Convers.*, vol. 37, no. 1, pp. 347–358, Mar. 2022.
- [115] G. Liu, H. Zhang, and X. Song, "Position-estimation deviation-suppression technology of PMSM combining phase self-compensation SMO and feedforward PLL," *IEEE J. Emerg. Sel. Topics Power Electron.*, vol. 9, no. 1, pp. 335–344, Feb. 2021.
- [116] S. Janardhanan and B. Bandyopadhyay, "On discretization of continuous-time terminal sliding mode," *IEEE Trans. Autom. Control*, vol. 51, no. 9, pp. 1532–1536, Sep. 2006.
- [117] G. Wang, X. Hao, N. Zhao, G. Zhang, and D. Xu, "Current sensor fault tolerant control strategy for encoderless PMSM drives based on single sliding mode observer," *IEEE Trans. Transp. Electrification*, vol. 6, no. 2, pp. 679–689, Jun. 2020.
- [118] G. Zhang, H. Zhou, G. Wang, C. Li, and D. Xu, "Current sensor fault-tolerant control for encoderless IPMSM drives based on current space vector error reconstruction," *IEEE J. Emerg. Sel. Topics Power Electron.*, vol. 8, no. 4, pp. 3658–3668, Dec. 2020.
- [119] A. T. Woldegiorgis, X. Ge, H. Wang, and M. Hassan, "A new frequency adaptive second-order disturbance observer for sensorless vector control of interior permanent magnet synchronous motor," *IEEE Trans. Ind. Electron.*, vol. 68, no. 12, pp. 11847–11857, Dec. 2021.



drives and controls.

**Ying Zuo** (Student Member, IEEE) received the B.Eng. degree in engineering from the Northwestern Polytechnical University, Xi'an, China, in 2018, and the M.S. degree in electronic engineering from the Institut National des Sciences Appliquées de Lyon, Villeurbanne, France, in 2019. She is currently working toward the Ph.D. degree in electrical engineering with the Department of Electrical and Computer Engineering, Concordia University, Montreal, QC, Canada.

Her research interests include electric machine



**Chunyan Lai** (Senior Member, IEEE) received the B.S. degree in engineering from the Sun Yat-sen University, Guangzhou, China, in 2010, and the Ph.D. degree in electrical engineering from the University of Windsor, Windsor, ON, Canada, in 2017.

She worked with the Midea Group, Foshan, China, between 2010 and 2013, and she worked as a Postdoctoral Fellow with the University of Windsor, between 2017 and 2018. She joined the Concordia University, Montreal, QC, Canada, in 2018, where she is currently an Associate Professor with the Department of

Electrical and Computer Engineering and a New Scholar Concordia University Research Chair on Transportation Electrification. Her research interests include electric motor drives and control, power electronics, vehicle to grid, and energy management systems.

Dr. Lai is an Associate Editor of the IEEE SYSTEMS JOURNAL.



**K. Lakshmi Varaha Iyer** (Senior Member, IEEE) received the B.Tech. degree in electronics and communication engineering from the SASTRA University, Thanjavur, India, in 2009, and the M.A.Sc. and Ph.D. degrees in electrical and computer engineering from the University of Windsor, Windsor, ON, Canada, in 2011 and 2016, respectively.

He is currently a Senior Manager with the Magna International's Corporate R&D Division. He is also an Adjunct Professor with the Department of Electrical and Computer Engineering, University of Windsor.

He has been innovating in the area of electric machines and power electronic systems for electrified automotive and renewable energy applications, since 2008. He has authored/coauthored more than 80 peer-reviewed papers in international conferences and journals and has authored/coauthored more than 30 patents.

Dr. Iyer was a recipient of the 2017 Governor General's Gold Medal in Canada and one among North America's "30 under 30" honored by Society of Manufacturing Engineers in 2018. He was also a recipient of NSERC CGS and OGS awards in 2014 during his doctoral studies at the University of Windsor. He is an Associate Editor of IEEE TRANSACTIONS ON POWER ELECTRONICS.